DOT-CG-N-02-86
DOT-TSC-CG-86-1

Medium-Frequency Data Link for Differential NAVSTAR/GPS Broadcasts

Boston University
Department of Electrical, Computer and
Systems Engineering
110 Cummington Street
Boston, MA 02215

June 1986
Final Report

Office of Navigation
Radionavigation Division
Washington DC 20593

Technical Report Documentation Page

1. Report No.	2. Government Accession No.	3. Recipient's Catalog No.
DOT-CG-N-02-86		

4. Title and Subtitle	5. Report Date
MEDIUM-FREQUENCY DATA LINK FOR DIFFERENTIAL NAVSTAR/GPS BROADCASTS	June 1986
	6. Performing Organization Code: DTS-52
7. Author(s): Per K. Enge, Michael F. Ruane, and Lee Sheynblatt	8. Performing Organization Report No.: DOT-TSC-CG-86-1
9. Performing Organization Name and Address: Boston University* Department of Electrical, Computer and Systems Engineering 110 Cummington Street Boston, MA 02215	10. Work Unit No. (TRAIS): CG672/B6013
	11. Contract or Grant No.: DTRS-57-85-C-00091
12. Sponsoring Agency Name and Address: U.S Department of Transportation United States Coast Guard Office of Navigation Washington, DC 20593	13. Type of Report and Period Covered: Final Report September 1985 - April 1986
	14. Sponsoring Agency Code: NRN-2

15. Supplementary Notes

*Under contract to: U.S. Department of Transportation
Research and Special Programs Administration
Transportation Systems Center
Cambridge, MA 02142

16. Abstract

Differential GPS must communicate differential corrections to civilian users of the Global Positioning System. Modulation of existing marine radiobeacons can provide the needed communication link for DGPS, provided the operation of existing radiobeacon direction finding equipment is maintained and adequate DGPS range is provided in the presence of atmospheric noise and skywave fading. Existing DF and ADF units were studied through a manufacturers' survey, and a radiobeacon modulation scheme has been proposed that maintains reliable DF and ADF operation. MSK modulation with a frequency offset of 325 Hz is recommended, with a power offset of -3dB. This scheme limits ADF bearing errors to under 3° based on analysis of the modulation energy entering the effective passbands of the various ADF designs. CCIR data on atmospheric noise and multipath were studied and a rate 1/2 convolutional code with constraint length 6 is recommended to provide a DGPS bit error probability of less than 10^{-5}. Reliable DGPS range for 10 nautical mile beacons will be 100 km, and for 30 nm beacons, 195 km. Discussion of interleaving to control atmospheric burst noise is included.

17. Key Words	18. Distribution Statement
Data Link, Differential GPS, Global Positioning System (GPS), Ground Wave Propagation, Marine Navigation, Medium Frequency, Radiobeacon, Radio Direction-Finding, Sky Wave Propagation	DOCUMENT IS AVAILABLE TO THE PUBLIC THROUGH THE NATIONAL TECHNICAL INFORMATION SERVICE, SPRINGFIELD, VIRGINIA 22161

19. Security Classif. (of this report)	20. Security Classif. (of this page)	21. No. of Pages	22. Price
UNCLASSIFIED	UNCLASSIFIED	96	

Form DOT F 1700.7 (8-72) Reproduction of completed page authorized

PREFACE

The work described in this report was performed under the University Research Program of the U.S. Department of Transportation. The Center for Navigation of the Transportation Systems Center directed the work, which was performed at Boston University's Department of Electrical, Computer and Systems Engineering. Funds were provided by the Radionavigation Division of the Office of Navigation, USCG, under the direction of LCDR Eric Erickson. This is the final report on Technical Task 1.

The authors wish to thank Rudy Kalafus and John Kraemer of the Transportation Systems Center for their encouragement and guidance. John Quill of the USCG Office of Research and Development, and David Pietrazewski, of the USCG Research and Development Center, provided helpful comments and suggestions throughout this effort. We also appreciate the cooperation of the technical representatives of the many manufacturers who provided information on their ADF hardware.

Contents

List of Figures

List of Tables

Chapter 1

Introduction and Summary

The objective of Technical Task No. 1 is to develop a marine-beacon based network for the communication of navigation related data to civilian users of the Global Positioning System (GPS). GPS is a worldwide satellite-based navigation system, currently being developed by the U.S. Department of Defense. It will include at least 18 satellites, all of which will broadcast ranging signals for many user communities. The accuracy of any user's position determination will be limited by the various error mechanisms which limit the accuracy of the range measurement. Some of these errors vary very quickly with time or space and cannot be treated with "differential" techniques. However, some vary rather slowly with time and space and can therefore be reduced by using a technique known as differential GPS (DGPS). Such errors include unmodelled ionospheric delay and "selective availability", which is introduced intentionally for the purpose of national defense.

A DGPS system includes a local reference station which uses a high quality GPS receiver to continuously measure range to all satellites in view. Since the reference station is fixed and its location has been surveyed, all slowly varying errors can be measured. Corrections for these errors can then be communicated via some suitable link to local users and these users can remove the errors from their range estimates. This procedure will improve the position fixing accuracy of the public GPS service from 100 meters to better than 20 meters.

Several communication links have been considered for the DGPS data. One proposed link adds a digitally modulated subcarrier to existing transmitters in the marine radiobeacon network. The frequency of the subcarrier is 0 to 500 Hz above the beacon's main carrier and the DGPS information is applied using either MSK or FSK modulation. This approach is attractive for the following reasons:

- A well located and widespread radiobeacon network is already in place, which means substantial site and equipment costs can be avoided.

Based on the analysis of these ADFs, MSK modulation with a frequency offset of 325 Hz is recommended. Additionally, a power offset of -3dB, a rate 1/2 error detecting and correction code are recommended.

A frequency offset of 325Hz is required to move the DGPS signal energy away from the "passbands" of the ADFs studied. A frequency offset of 0 Hz is not recommended for 3 reasons. First of all, some aviation ADFs use coherent detection and these detectors develop a coherent reference by phase tracking the radio beacon carrier. DGPS energy at 0 Hz could introduce unacceptably large levels of phase jitter at the phase lock loop output. Secondly, the DGPS bandwidth is relatively wide (even if MSK modulation is used) and could interfere with the operation of ADFs having small switching frequencies. (Switching signals are explained in Chapter 2.) Finally, the ADF switching signals will modulate DGPS at 0Hz directly into the passbands of the detectors. This will produce unacceptably large noise in the bearing estimates.

A frequency offset of 325Hz does not yield appreciable DGPS interference from the neighbor beacons, because of the 15 dB protection ratio. The rate 1/2 error correcting code "spreads" the spectrum of the DGPS signal relative to all ADF passbands and hence reduces interference effects. The error correcting code also greatly increases the DGPS range as discussed below. CPFSK cannot be used even though it spreads the DGPS energy over a wider spectrum. CPFSK has 2/3 of its energy at two discrete frequencies, and can produce severe bearing errors whenever the discrete frequencies enter an ADF passband.

Subtask No. 2 studies the effect of atmospheric noise and multipath on the performance of the DGPS link. Atmospheric noise and skywave (MF multipath) are described in CCIR Reports and this information was stored in a computer data base for use in analysis. Atmospheric noise is impulsive and therefore motivates the combined use of limiting or clipping in the receiver and error detecting and correcting (EDAC) codes. The probability of DGPS bit error ($Pr(\epsilon)$) is computed for such receivers and a variety of codes. These curves reveal that significant performance improvements are achieved if codes of moderate complexity are used. Specifically, convolutional codes of rates 1/2 and 2/3 are analyzed. These codes both have constraint lengths (v) of 6, where constraint length roughly measures decoder complexity and data latency. The signal to noise ratio required for $Pr(\epsilon) \leq 10^{-5}$ is 31, 12 and 6 dB for uncoded, rate 2/3-coded, and rate 1/2-coded systems, respectively.

Probability of link availability is defined as the probability that the SNR required for $Pr(\epsilon) \leq 10^{-5}$ will be achieved. The atmospheric noise and skywave data bases were used to compute $Pr(\textit{link available})$ as a function of range away from the beacon. The following results were obtained for the noisiest time block in Boston, Massachusetts. A link without coding and with a 30 nautical mile beacon will be available with probability .9 if the user

Chapter 2

Modulation Scheme

2.1 Modulating Radiobeacons for DGPS

In this section, we evaluate the impact of various DGPS modulation schemes on the performance of existing DF equipment. Key assumptions underlying the analysis are presented first, followed by possible alternative modulation schemes. The status of DF and automatic direction finding (ADF) equipment will be considered next, based upon a survey of manufacturers of both marine and aeronautical units. It is argued that manual DF units are insensitive to DGPS modulation and we concentrate on a taxonomy of ADF technologies. Finally a general analysis method is described that yields the parameters required for DGPS modulation to ensure aceptable DF service by a given class of ADF receivers. Based on these requirements, the following recommendations are made:

- Modulation should be MSK.
- DGPS carrier offset should be 325 Hz.
- DGPS amplitude should be -3dB from the main carrier.
- A rate 1/2 error correcting code should be incorporated.

2.2 Key Assumptions

In the absence of a program of bench testing, and faced with limited details about many ADF units, a model-based analysis of interference effects was performed. To ensure that degradation of service would be detected in such an analysis, a number of conservative, worst-case assumptions were employed. This allowed recommedations to be based on ADF designs most sensitive to DGPS interference, even if the complete description of such units was unavailable.

m or for non-integer m have even boader spectra than MSK or CPFSK(m=1) but offer possible receiver cost differentials. These cost advantages are already small in comparison with total unit costs, and are expected to disappear by the time GPS becomes operational. Other classes of modulation such as QPSK, or PSK have broader spectra as well. PSD's of MSK and CPFSK(m=1) are shown in Figures 2.1 and 2.2 for symbol rates of 75 and 100.

A bit rate of 50 bps is required for the DGPS signal, but error detection and correcting codes will increase the channel symbol rate to 75 or 100 symbols per second. The PSD's in Figures 2.1 and 2.2 are normalized to 1 to show the relative spreading of CPFSK compared to MSK, and to show the spreading due to increasing the symbol rate. In addition, note the discrete components in CPFSK at $f_d = B/2$.

The DGPS protection ratio is the ratio of radiated DGPS power compared to radiated beacon carrier power. DGPS protection ratios of -3dB and -6dB are considered.

An adjacent beacon having DGPS modulation is assumed, giving rise to Figure 2.3. As shown, the carriers are separated by 1000Hz, the minimum USA spacing, and the adjacent beacon is 15dB below the beacon being used for bearing. Each has an MSK modulated signal offset by the subcarrier and 3dB down from the carrier. The adjacent beacon DGPS is therefore at -18dB. In Europe, beacon spacing of 500Hz has been proposed.

The general nature of interference possibilities can be explained from Figure 2.3. There can be self-beacon or adjacent beacon interference. Self-beacon interference arises because ADF operation depends on detection of signals in sidebands located within a few hundred Hz of the beacon carrier. With small offset, f_{DGPS}, the DGPS spectrum overlaps and corrupts signals near the carrier. A narrower DGPS spectrum delays the onset of interference as f_{DGPS} decreases, but eventually some f_{DGPS} is reached with substantial DGPS energy reaching the ADF.

Increasing f_{DGPS} avoids these problems for self-beacon interference but simultaneously moves the DGPS spectrum of the adjacent beacon towards its higher frequency neighboring beacon. If f_{DGPS} becomes too large, adjacent beacon DGPS power will reach the ADF. The narrowness of the DGPS spectrum and the protection ratios for DGPS and adjacent beacons limit the interference effects.

Table 2.1 below summarizes the modulation scheme parameters that were analyzed.

2.4 Manual DF User Equipment

Manual DF equipment is quite similar to the ADF equipment described in the next section. Rather than automatically finding the bearing, manual DF equipment instead produces an audible tone or meter display whose magnitude indicates bearing error. The user manually

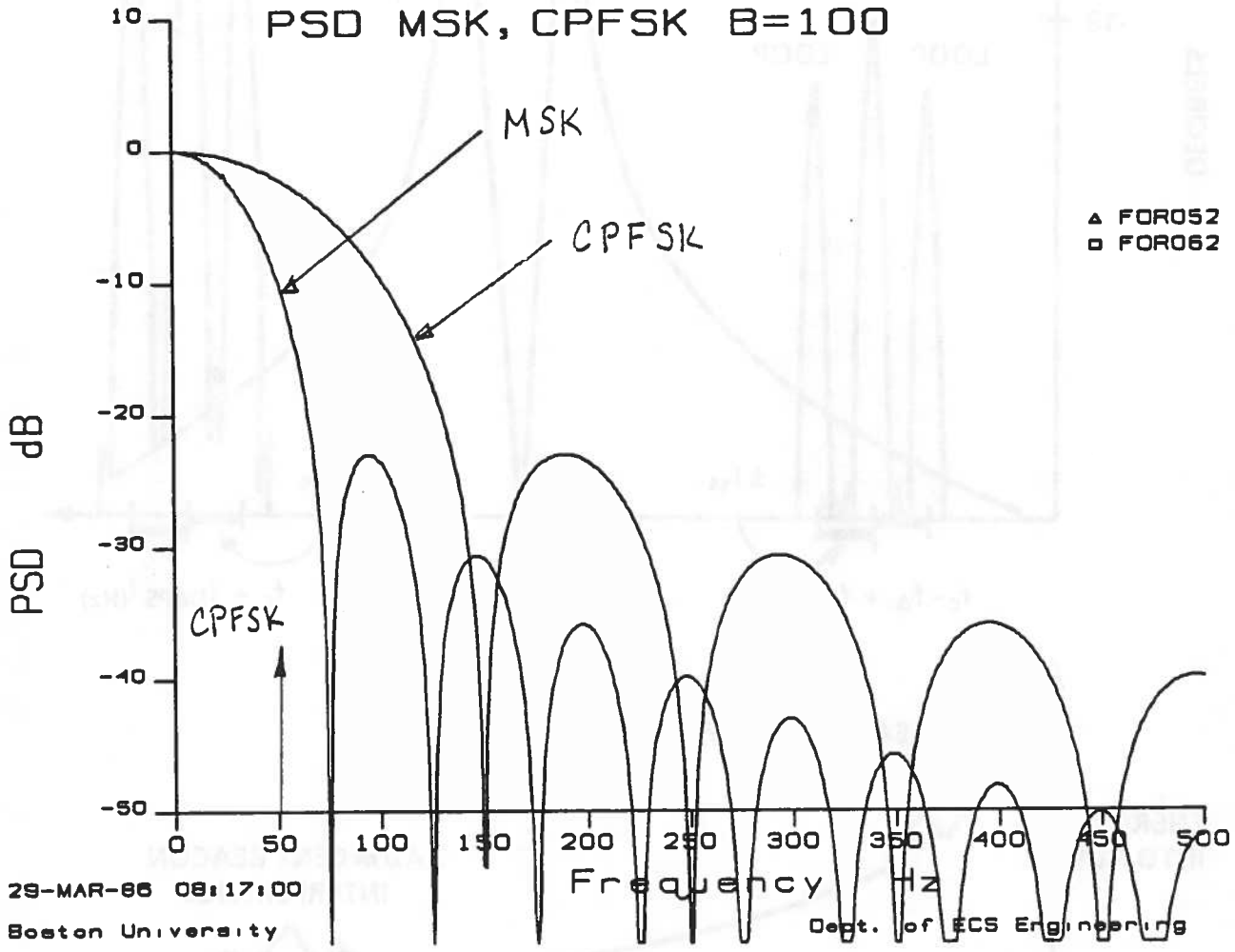

Figure 2.2: Power Spectral Densities at B=100

Table 2.1: Modulation Variables

DESIGN CHOICE	OPTIONS CONSIDERED
Type of Modulation	MSK or CPFSK(M=1)
DGPS Protection Ratio	-3dB
Adjacent Beacon Protection Ratio	-15dB
Adjacent DGPS Protection Ratio	-18dB
Adjacent Beacon Spacing	1000 and 500
Offset of DGPS (f_{DGPS})	0 to 500 Hz
Error Correcting Codes	rate 1/2 or rate 2/3

rotates the antenna until a null is reached and the tone disappears.

Interference from DGPS will appear in a manual DF unit as modulation of the tone or meter signal. The overall function of the unit will not change although a true aural null might be impossible with DGPS noise being present. While experienced users may notice the different sound of their DF, DGPS is not expected to contribute to bearing error except in weak signal regions where it might be difficult to detect the aural null of the beacon compared to the DGPS noise. Because of DGPS's expected minor impact on manual DF performance, and the difficulty of assessing that impact quantitatively in a technology strongly dependent on user experience, we conclude that manual DF interference will not determine the design of the DGPS modulation scheme. Manual DF's will not be considered further.

2.5 Characterization of ADF User Equipment

Over 110 companies that were possible marine or aeronautical ADF manufacturers and distributers were contacted. Of the original list, 16 companies claimed to be active independent suppliers of ADF equipment in the radiobeacon band. These were contacted a second time with a detailed request for information about their units. Only 14 offered ADFs (the other two had only manual units), and information was received for 20 different models. We estimate, from indirect references in sales materials, that at least another 5 or 6 models are offered by these companies, but no information was provided on those units.

The quality of the information varied greatly. Several companies provided technical manuals with block diagrams, theory of operation, and schematics. Others provided instuction booklets intended for non-technical users. A few supplied only data sheets and promotional descriptions. One company responded with a brief letter mentioning that they offer several ADFs, but provided no documentation or descriptions. Finally, a few companies forwarded our detailed requests to overseas engineering offices in Europe and

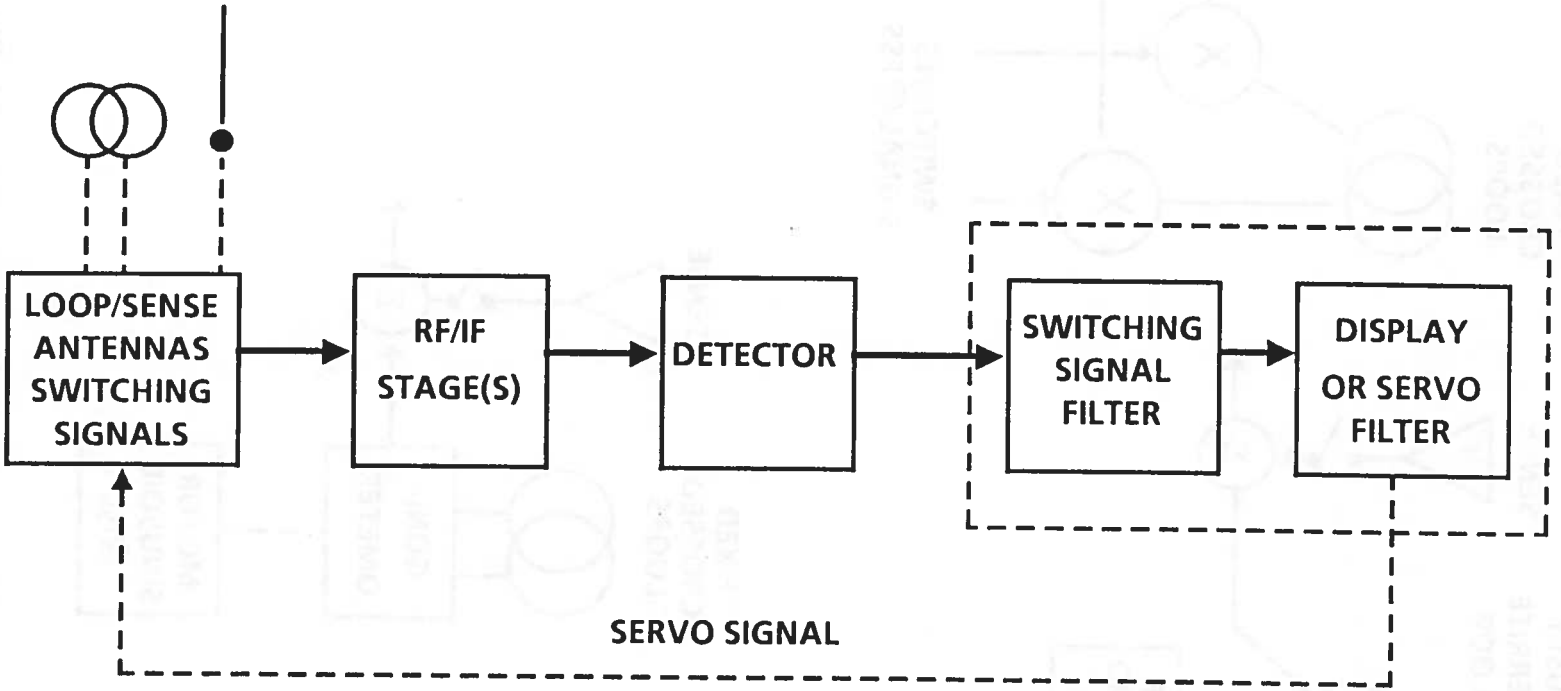

Figure 2.4: Interference Oriented Block Diagram for ADFs

determines f_{SS} while the phase ϕ is the angle to the beacon compared to some fixed reference position of the rod, e.g. the ship's centerline. Here the switching signal is sinusoidal and the signal is of the form $\cos(2\pi f_{SS}t + \phi)$. The upper right design uses fixed crossed loops, with each loop output, $\cos\phi$ and $\sin\phi$, being multiplied by quadrature switching signals, $\cos(2\pi f_{SS}t)$ and $\sin(2\pi f_{SS}t)$. Once again the signal is of the form $\cos(2\pi f_{SS}t + \phi)$. In the lower example, the goniometer serves to recreate the field configuration at the antenna within the goniometer coils. A rotating search coil within the goniometer functions just like the rotating ferrite rod or loop, but has the advantage of allowing fixed antenna equipment. The signal f_{SS} is determined by the motor speed. In all these examples, the sense antenna is switched on when ambiguity must be resolved. Note that all these signals are modulating the carrier, and will appear as sidebands offset by f_{SS}.

Figure 2.6 shows antenna configurations where bearing information is carried by the magnitude. At the left a fixed crossed loop antenna and goniometer are used to recreate the beacon field in the search coil. Letting ϕ be the bearing angle error in this system, the search coil determines the magnitude of the received carrier according to $A\sin\phi$. The switching signal multiplies the carrier to create sidebands at $\pm f_{SS}$ whose magnitude reflects the bearing error. The sense is usually connected in such systems to resolve the ambiguity. Since loop signals and sense signals are generated by the H and E fields of the received beacon, respectively, the sense is sometimes shifted another 90° and added to the loop signal. The summed signal now varies between 0 (sense and maximum bearing error signal cancel due to 180° phase difference and same amplitude) and A (sense only since loop magnitude goes to 0 at true bearing). The right hand system is similar, except the sense is switched at f_{SS} in addition to phase shifting.

For interference analysis, the key characteristics of an antenna configuration are:

1. Is bearing information in phase or magnitude?
2. Is the sense always connected?
3. Is switching signal applied to loop or sense?
4. Is the switching signal sinusoidal or square?
5. What is f_{SS}?

2.5.3 RF/IF Stages

ADFs employ a variety of designs in their RF and IF stages. Bandlimiting may be done in a number of locations and more than one IF stage is used in some units. Many units are suited for reception of signals from several bands, including commercial broadcast stations,

emergency beacons and aeronautical beacons, and utilize a switchable bandwidth. The most common intermediate frequency was 455kHz.

Our interference analysis only requires knowledge of the overall IF passband. While a few units claimed IF -6dB points of ±1000Hz or less, most fell in the range of ±2kHz to ±4kHz for -6dB points. The -60dB points available were on the order of ±10kHz. Our conclusion is that the RF/IF stage will pass all the DGPS energy, and need not be considered in detail.

2.5.4 Detector

The detector block functions to bring the output of the RF/IF stages back to baseband. The detector could be determined in 14 of the ADFs studied; in 10 units a non-coherent AM detector was employed. Four units, all of which were avionics models, used coherent detection.

The non-coherent detectors can be thought of as simple low pass filters that extract the signal at f_{SS} and block higher frequencies. Some protection against DGPS interference would occur here if DGPS is well above the cutoff of the detector. However, most detectors appear to have been designed primarily to eliminate beacon tones or adjacent beacons, and have wide passbands compared to f_{SS}.

Coherent detectors in avionics ADFs relied on phase-locked loops to extract the reference phase from the carrier signal. While these designs provide improved performance at low signal-to-noise levels, they can be vulnerable to several DGPS-induced problems. See Figure 2.7.

The phase-locked loop consists of a mixer that multiplies the incoming signal and the signal of the voltage controlled oscillator. Normally the incoming signal is

$$s(t) = \cos(2\pi f_c t + \theta)$$

where f_c is the beacon carrier. The VCO operates at $\sin(2\pi f_c t + \hat{\theta})$ such that their product is

$$e(t) = \cos(2\pi f_c t + \theta)\sin(2\pi f_c t + \hat{\theta})$$

or

$$e(t) = [\frac{1}{2}\sin 2(\hat{\theta} - \theta) + \frac{1}{2}\sin(4\pi f_c t + 2\hat{\theta} + 2\theta])$$

This signal then passes through the low pass filter, eliminating the $2f_c$ term and producing a signal proportional to the phase error, $\hat{\theta} - \theta$. When $\hat{\theta} - \theta$ is small, $\sin(\hat{\theta} - \theta)$ is approximated by $\hat{\theta} - \theta$ and the loop can be analyzed as a linear system. This corresponds to the 'locked' condition. When 'unlocked', the $\sin(\hat{\theta} - \theta)$ term must be considered and a nonlinear system results.

The modulation schemes under consideration use continuous phase changes to represent information, and have the potential to cause false lock or PLL unlock. Unfortunately the available information on ADF PLLs is insufficient to allow a detailed analysis of the nonlinear noise effects of DGPS on the phase estimate. In general, it is extremely difficult to analyze nonlinear PLL operation in the presence of noise, even with detailed knowledge of the PLL design [18]. PLL unlock can best be avoided by locating DGPS far enough from ADF filter passbands to ensure no PLL interference effects.

A false lock could occur if DGPS carrier were mistaken for the carrier of the PLL during pull-in. This would depend on the relative signal levels of DGPS and the beacon carrier and the acquisition characteristics of the PLL. PLLs are specified to have some 'lock-in range' over which they will locate and lock on a signal. For the ADFs we studied, this range was on the order of $\pm$250Hz to $\pm$300Hz. If DGPS were locked, the PLL output would no longer be coherent with the bearing signal and bearing error would result. Two units had 'lock detector' circuits that effectively shut off the ADF function whenever the frequency difference between the oscillator and the RF/IF input exceeded 10Hz. These same units had 100Hz cutoffs on their PLL low pass filter.

Unlock due to a 10Hz difference might occur when DGPS contributed a string of 1's or 0's, producing a progressive phase change. For example, at a bit rate of 100 bps, and 90° shift per bit, a string of similar bits appears as a 25Hz modulation. This 25Hz modulation might create jitter in the bearing estimate, or it might be interpreted as an unlock condition, causing the lock detector to operate. The loop would then try to resynchronize. This situation could cause noticeable jitter in the bearing estimates.

Another PLL unit warned of such jitter when locking on weak stations. That unit controlled the loop antenna from the lock detector. When unlocked, the loop is disabled and the signal is acquired from the sense antenna only. When locked, the loop is enabled so ADF can begin. If, for a weak station, the extra noise introduced by the loop causes unlock, the unit will audibly click on and off as the loop is enabled and disabled repeatedly. The manufacturer suggests tuning another frequency to resolve the problem. No data is available as to the relative signal-to-noise ratio required to prevent this problem.

Key characteristics for interference analysis are

1. Is the detector coherent or non-coherent?
2. What is the bandwidth of coherent loop filter?
3. What is the bandwidth of the non-coherent detector?
4. What is lock-in range for a PLL?

2.5.6 Servo/Display Filter

The last generic block concerns the display of the bearing information. While conceptually important, this block was the least well described by technical materials on the ADFs, and will be considered part of the switching signal filter.

Generally the bearing is shown by electrical or mechanical displacement of an indicator. Most servos move an arrow or compass card against a reference circle to show bearing with respect to the ship or aircraft centerline. These devices must remove the ambiguity as part of the display. Units with CRT displays create a 'propeller' shape that is oriented in the true bearing direction and at 180° from true bearing. Enabling the sense blocks part of the display and removes ambiguity. Digital readouts gave bearing directly, while LED arrays gave readings to 5° steps around the compass. Claimed bearing accuracies were from ±0.5° to over ±5°.

On most units, the servomotor is used for both switching signal filtering and display. The indicator would be directly attached to the shaft, and the last two blocks of the generic ADF are quite naturally combined. Virtually no data was obtained to allow separation of these functions for servomotors. Similarly, no information was available for characterizing the digital and LED displays. CRT's have no appreciable dynamics in representing the ADF switching filter outputs.

2.5.7 Taxonomy of ADF Approaches

From the perspective of interference analysis, ADFs we reviewed can be placed into 5 groups, described by their switching signal (f_{SS} and waveform), their detection method (coherent or non-coherent), and their switching filter/display methods (servo, CRT, or digital). Not all combinations were found. Though we were not able to determine the design of all 20 units, 14 were described in sufficient detail for classification, and the others have been assigned based on similar units. The categories include:

1. Sinusoidal, coherent detection, servomotor (4)
2. Sinusoidal, noncoherent, servomotor (7)
3. Sinusoidal, noncoherent, CRT (6)
4. Square wave, noncoherent, servo (2)
5. Square wave, noncoherent, digital (1)

One unit had both CRT and servomotor display, but was placed in a servo category since that determines the switching filter characteristics. Figure 2.8 shows the distribution of units in each category versus f_{SS}.

2.6 Motor Analysis

Servomotor systems were the most common ADF design used both for detecting and displaying the bearing angle. Despite employing a variety of antenna and goniometer configurations, modulation and detection schemes, and display devices, servomotor ADFs all shared a common system structure. The received signal bearing is transformed to either magnitude or phase information at the switching signal frequency. Passing through RF and IF stages, this information is eventually detected and applied as a control voltage to the servomotor. In all units but one, a two phase AC induction motor was used. Two phase induction motor servos are widely used for position control, and here serve to alter the effective antenna position. On units with fixed crossed loop antennas and goniometers, the servo merely rotates the goniometer search coil; on units with ferrite rod antennas, the rod itself is rotated. Rotation of the goniometer search coil or ferrite rod changes the received signal and eventually the control voltage. As the antenna bearing approaches the true bearing of the received signal, the control voltage decreases. At the true bearing the control voltage goes to zero and the servo stops. Usually the bearing indicator is mounted on the same shaft as the goniometer search coil. For ferrite rod antennas, the display usually surrounds the antenna mount. The bearing readings therefore approach the true bearing with a time constant determined by the motor/shaft combination.

Two phase AC servomotors [20] typically have a reference phase voltage at sinusoidal frequency f_r that establishes a rotating flux field. The control phase sinusoidal voltage, also at f_r but usually phase shifted 90°, creates its own flux field that couples with the reference phase flux field to produce mechanical torque. When the voltages of the two phases are balanced, no torque is developed. Control voltages above or below the reference magnitude produce torque in one direction or the other. Servomotors have good stability characteristics, due to their very high rotor resistance which causes their torque-speed curve to be negative.

To understand the dynamic performance of AC servomotors we must consider three factors. First, the servomotor loses net torque when the control phase frequency differs from the reference phase frequency. Because developed torque depends on coupling two rotating fields, the coupled fields actually create a pulsating torque (always in the same direction) at the reference phase frequency. In many common servo applications, f_r = 400Hz. In ADFs, f_r ranged from 32Hz to 200Hz with most values about 100Hz to 135Hz. This pulsating torque encounters the motor mechanical damping which has a time constant on the order of τ_m = 0.5 sec, so that only the DC component of the pulsating torque is seen. Servomotors therefore can be considered as a mechanical form of coherent detector.

Second, there are two quite different time constants in servomotors. The first is the mechanical τ_m. Typically this ranges between 0.5 sec and 1 sec. Although no direct data

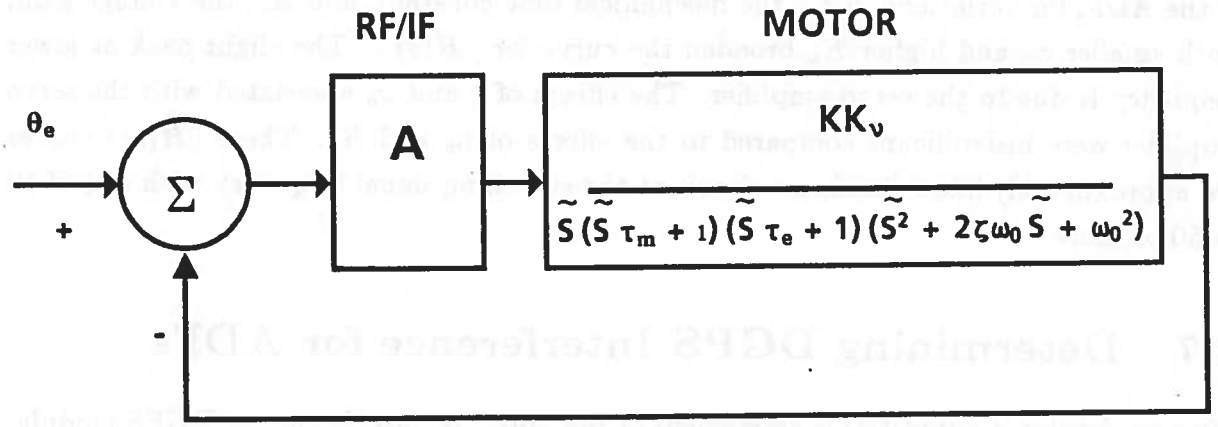

Figure 2.10: ADF Servo System Model

as a phase or magnitude, depending on the particular ADF. The error passes through the RF/IF stages and is detected in the first block. Since the RF/IF stages typically have passbands of several kHz, it is assumed that their total effect on the bearing error is a gain, A. The second block is the motor from Figure 2.9. The motor output is a displacement angle $\hat{\theta}$ that represents the rotation of the antenna. The objective of the servo system is to drive the bearing error, θ_e to zero. Due to the mechanical system associated with display of the bearing, the correct bearing is displayed when θ_e is zero,. The unity negative feedback represents the direct coupling seen in most units between motor position and antenna position.

The closed loop transfer function of Figure 2.10 can be written as:

$$H(s) = \frac{AKK_v}{\tilde{s}(\tilde{s}\tau_m + 1)(\tilde{s}\tau_e + 1)(s^2 + 2\zeta\omega_o s + \omega_o^2) + AKK_v}$$

where

$$\tilde{s} = j(|\ \omega - \omega_r\ |)$$

and

$$s = j\omega$$

The distinction of $\tilde{s}$ and s reflects the coherent behavior of the servomotor. Motor dynamics are determined by frequency variations about the reference f_r, or equivalently,

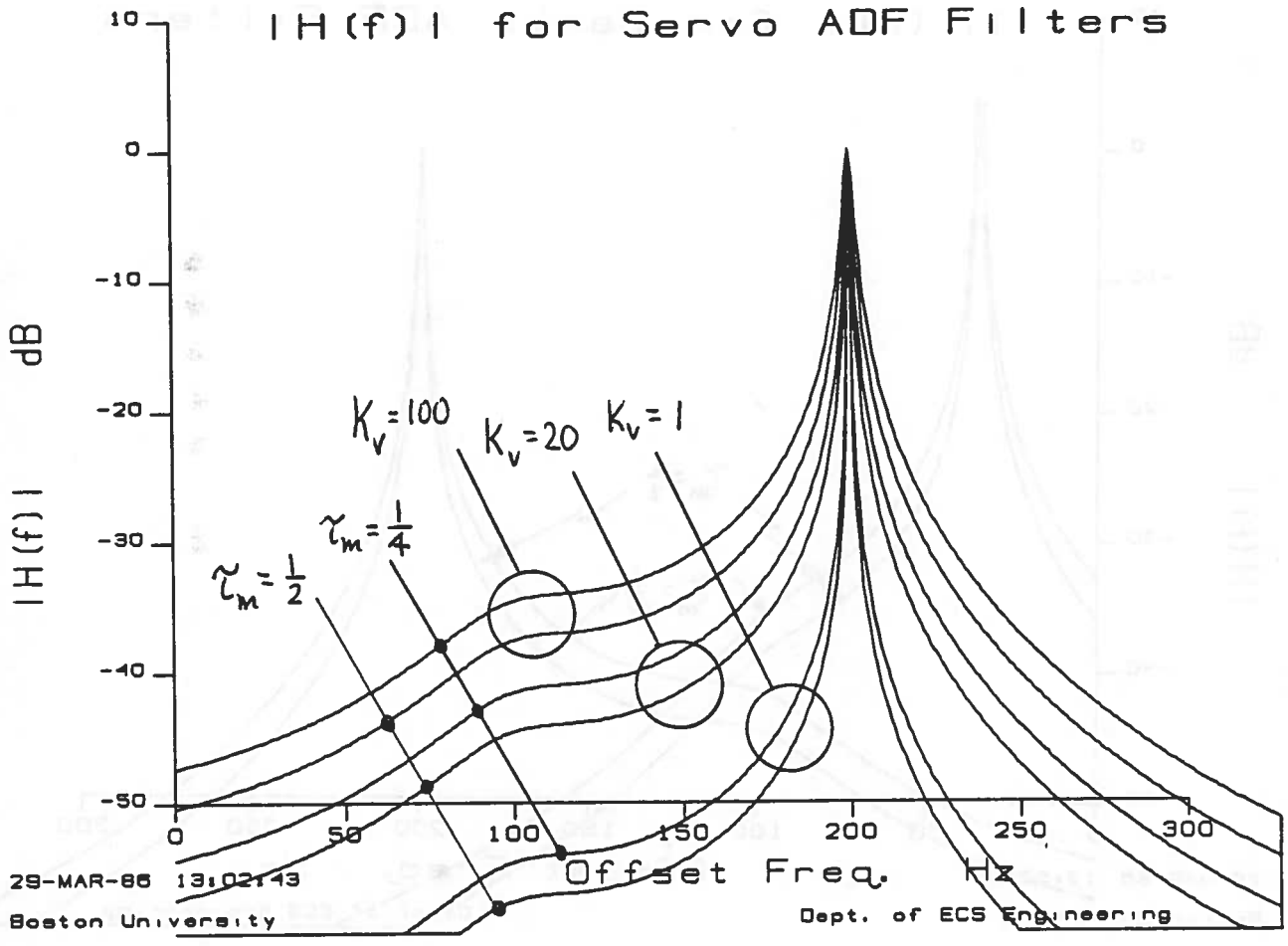

Figure 2.11: Frequency Response of Closed Loop Servo

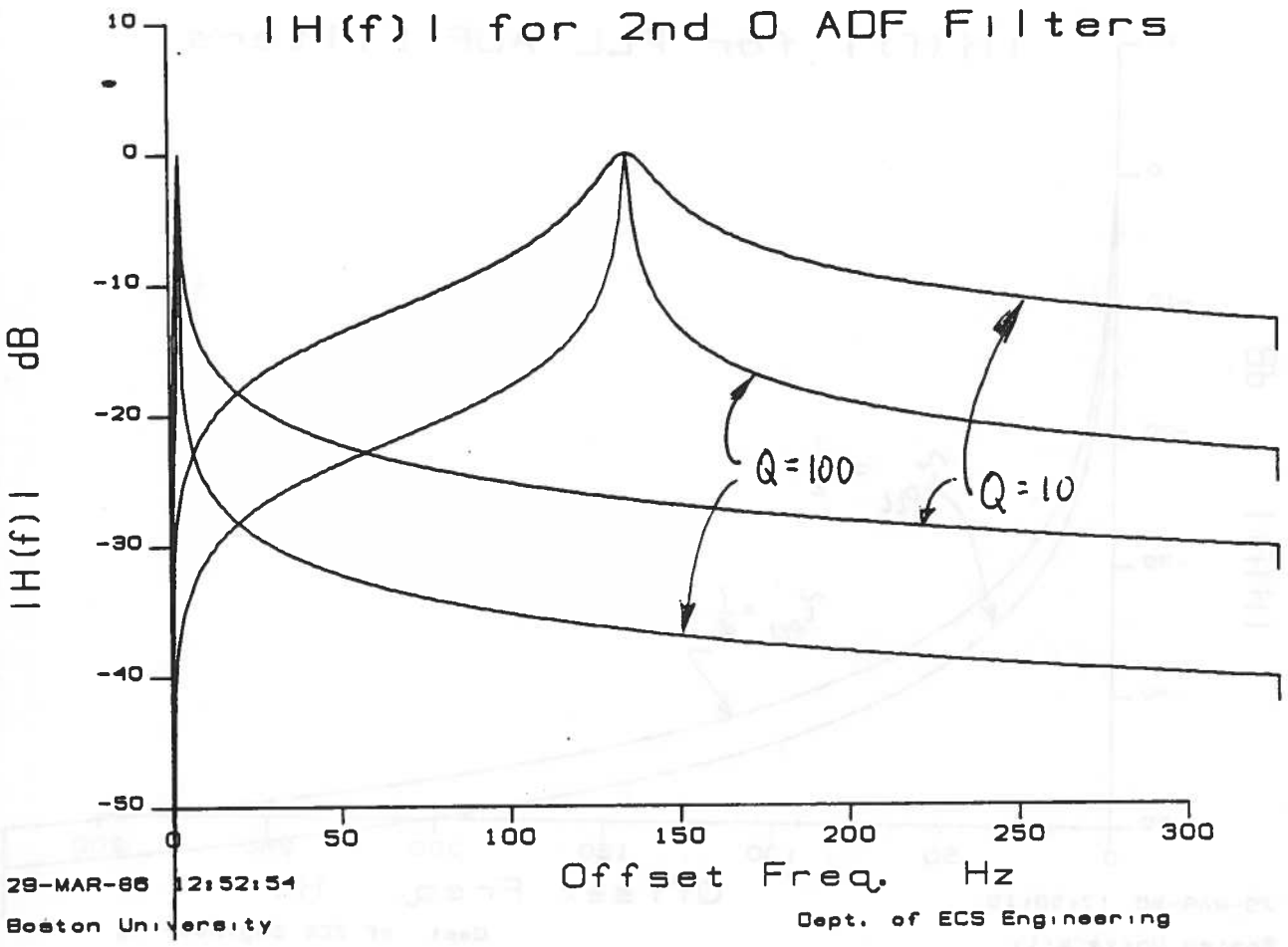

Figure 2.13: Passbands for Second Order ADFs

Figure 2.14 represents the coherent detectors. The coherent units all had phase locked loops at the carrier frequency to detect either magnitude of phase information on bearing. As discussed earlier, the linear performance of these systems is like a very narrow filter about the carrier. We approximate this by a low pass filter with a cutoff of either 2Hz or 4Hz. In some coherent detection units using amplitude modulation, the PLL is cascaded with a synchronous filter. The one unit with sufficient detail to describe the synchronous filter had a cutoff of about 2Hz around the switching signal. We have cascaded our low pass PLL filter with a 2Hz synchronous filter in both curves. This representation cannot describe the unlock conditions of the PLL, but does approximate the normal operation of the coherent ADFs.

These passbands bound the performance of all the units we have studied. Modulation decisions that do not affect these extreme units should provide satisfactory performance for units at intervening frequencies and with filter parameters similar to those we have been able to examine in detail.

Qualitative assessment of competing modulation schemes can begin with these passbands and the previous diagrams of MSK and CPFSK spectra. For example, it is apparent that offsetting the DGPS signal in the 0 to 200Hz range could lead to interference by allowing DGPS energy to enter the passbands of some units. At the 0Hz end, the coherent detectors would be vulnerable to unlock, and non-coherent units with f_{SS} in the area of 35Hz to 90Hz could be affected. At offsets near 135Hz, several servo and CRT units would be vulnerable. Increasing offset above 200Hz increasingly removes the danger of interference, although it is desirable to keep offset low to avoid adjacent beacon effects. The single unit found at $f_{SS} = 200Hz$ does not seem to play any significant role in the ADF market. It is a ferrite rod marine unit, and is apparently no longer in production. Designed in Japan, there is a domestic company distributing literature on the unit, but they cannot provide engineering support or information. Below this unit, there are next a number of ADFs at f_{SS} =135Hz; therefore we will consider a passband at 135Hz to be the critical upper passband in our remaining analysis.

2.7.2 Interference Spectra

In this section we begin to quantify the significant mechanisms determining the exact nature of interference. This will allow us to replace the above qualitative arguments with quantitative measures of interference. The resulting recommendation about DGPS modulation will be based on this quantitative analysis and some inescapable qualitative concerns dictated by our conservative approach and the uncertainties around issues like PLL unlock in coherent detectors.

Because the switching signal of the ADF modulates DGPS as well as the beacon, inter-

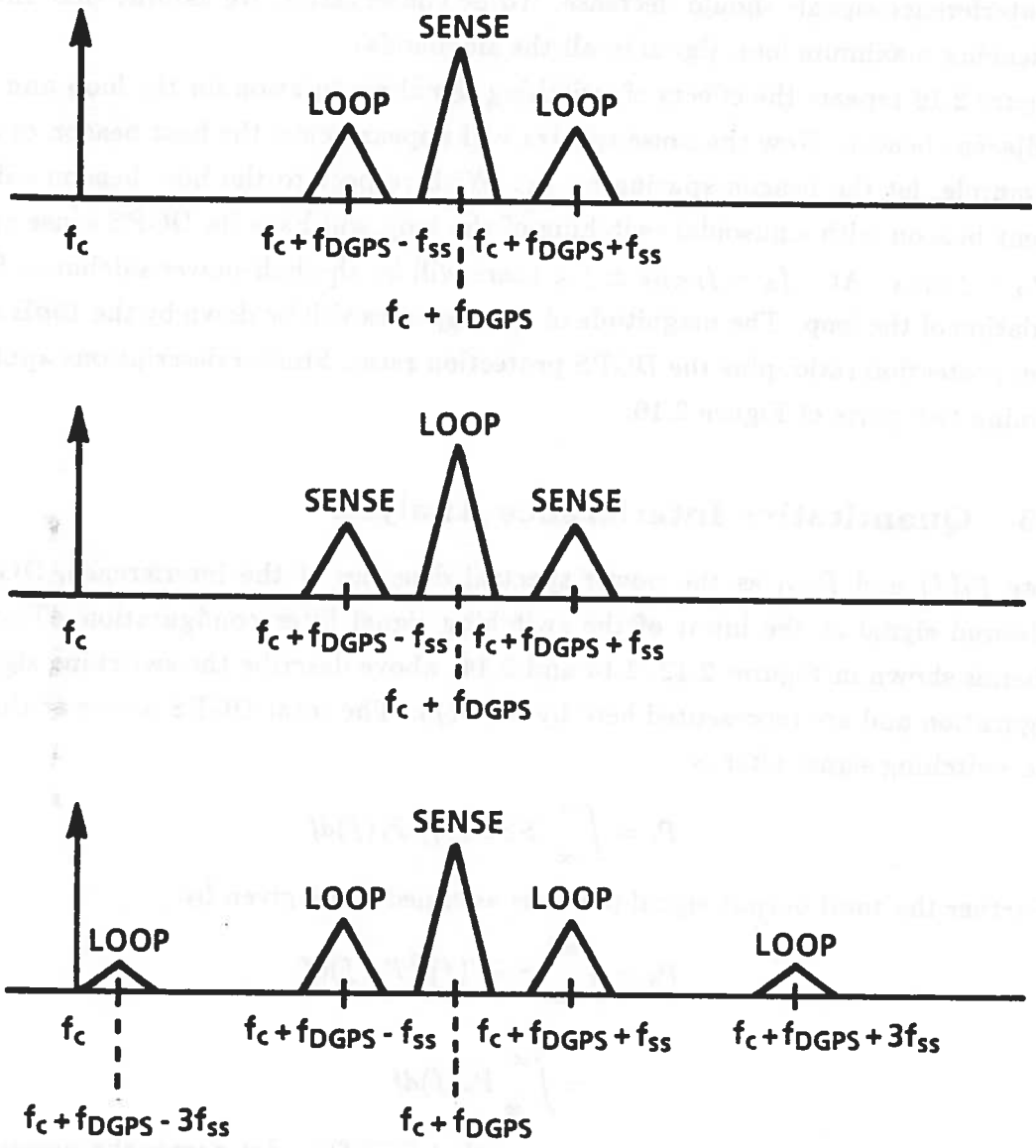

Figure 2.15: Host Beacon Switching Signal Effects

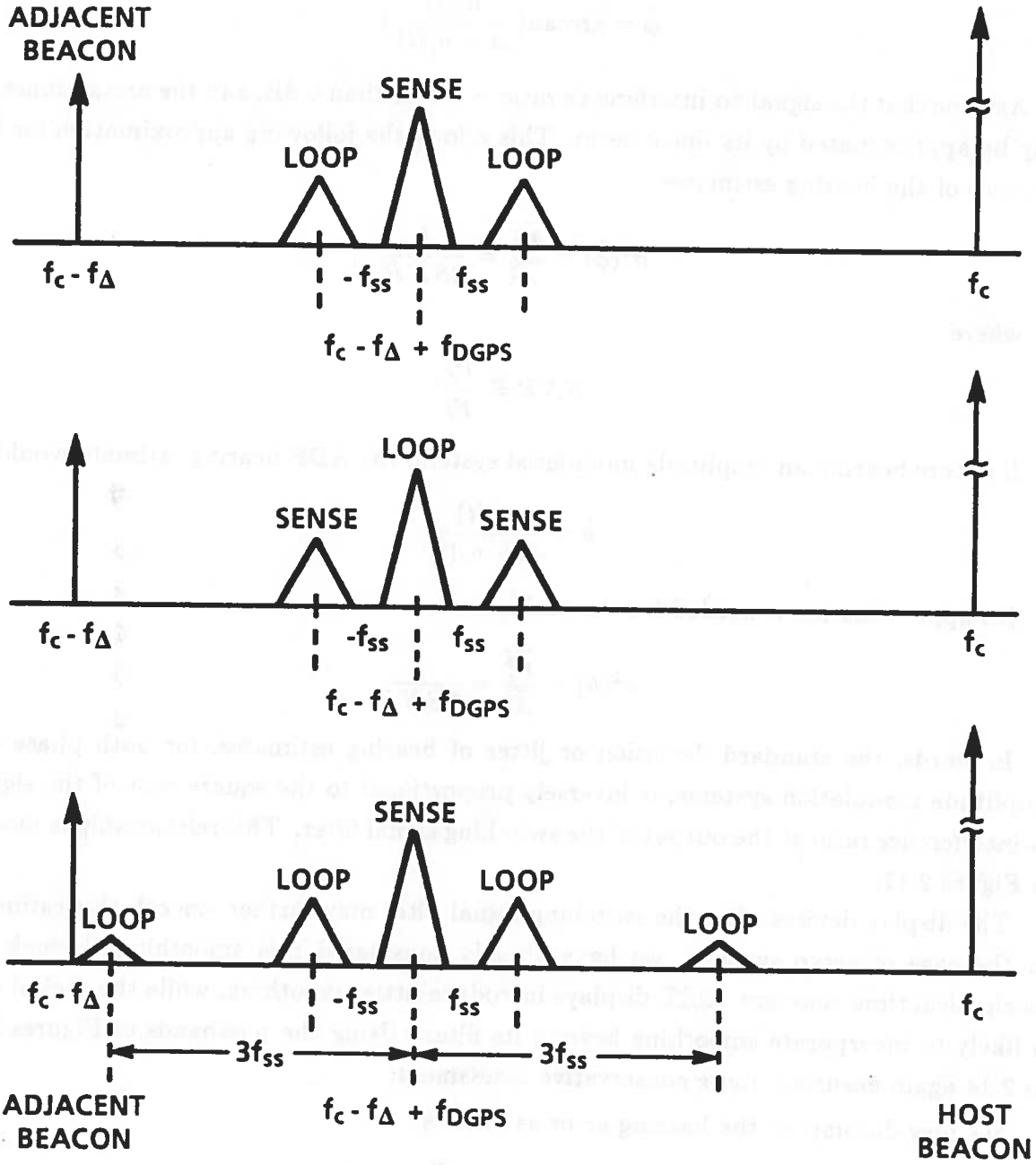

Figure 2.16: Adjacent Beacon Switching Effects on DGPS

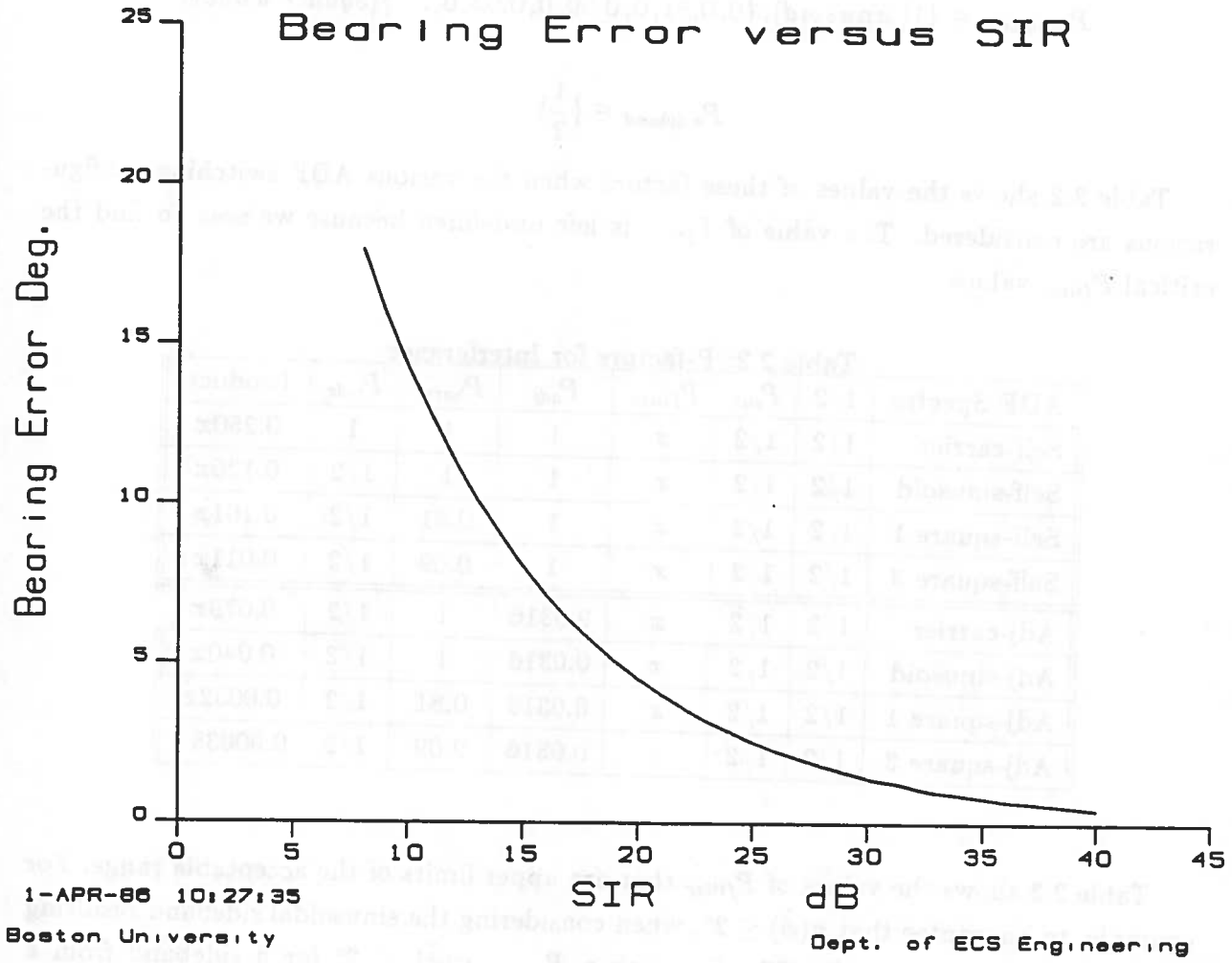

Figure 2.17: Bearing Error vs. SIR

Table 2.3: P_{filter} Values for Bearing Error

ADF Spectra	3^o	2^o	1^o
Self-carrier	0.0110	0.0049	0.0012
Self-sinusoid	0.0219	0.0097	0.0024
Self-square 1	0.0271	0.0121	0.0030
Self-square 3	0.2492	0.1108	0.0277
Adj-carrier	0.3481	0.1551	0.03797
Adj-sinusoid	0.6931	0.3070	0.0760
Adj-square 1	0.8576	0.3829	0.0949
Adj-square 3	7.8861	3.5063	0.8765

$$SIR = \frac{P_I}{P_S} = \frac{\int_{-\infty}^{\infty} |SSF(f)|^2 P_I(f) df}{\int_{-\infty}^{\infty} P_S(F) dF}$$

where P_I is MSK. Figure 2.21 shows the results for a second order filter when P_I is CPFSK(m=1). Note that the CPFSK discrete frequencies cause a peak in the energy entering a passband when the DGPS offset corresponds to $B/2$. The peak should be on the order of $1/3$, since that is the energy in the discrete components. This is reduced somewhat since the passband value must be considered. The clipped shape of the Q=100 curves is an artifact of the integration and plotting step sizes. It is also clear how the higher symbol rate spreads the MSK spectrum and produces a smaller P_{filter} at low offsets. However, at larger separations, the higher symbol rate modulation has more energy in its sidelobes, and P_{filter} is greater. Comparing the motor curves with the PLL curves indicates servo and PLL ADFs are similar in their interference behavior. In fact, since most PLL units also have a servomotor display and/or a digital filter, the PLL performance will generally be better than the simple motor switching filter configurations. The PLL- servomotor combination is not reflected in these figures. High Q second order ADFs are similar to motor and PLL systems as well. Only low Q units show dramatically higher vulnerability to noise effects.

As DGPS offset increases, the train of spectra consisting of the DGPS spectrum at the DGPS carrier and its sinusoidal or squarewave sidebands, slide across the various passbands we have shown. We seek a value of f_{DGPS} that will prevent unacceptably large bearing errors in any ADFs. For any particular ADF, as f_{DGPS} increases, there will be a series of peaks in $\sigma(\hat{\phi})$ as successive self beacon sidebands pass through the ADF passband. At very large f_{DGPS}, the adjacent beacon sideband and DGPS carrier spectra cause another series of peaks in $\sigma(\hat{\phi})$, but with considerably lower magnitude due to the adjacent beacon

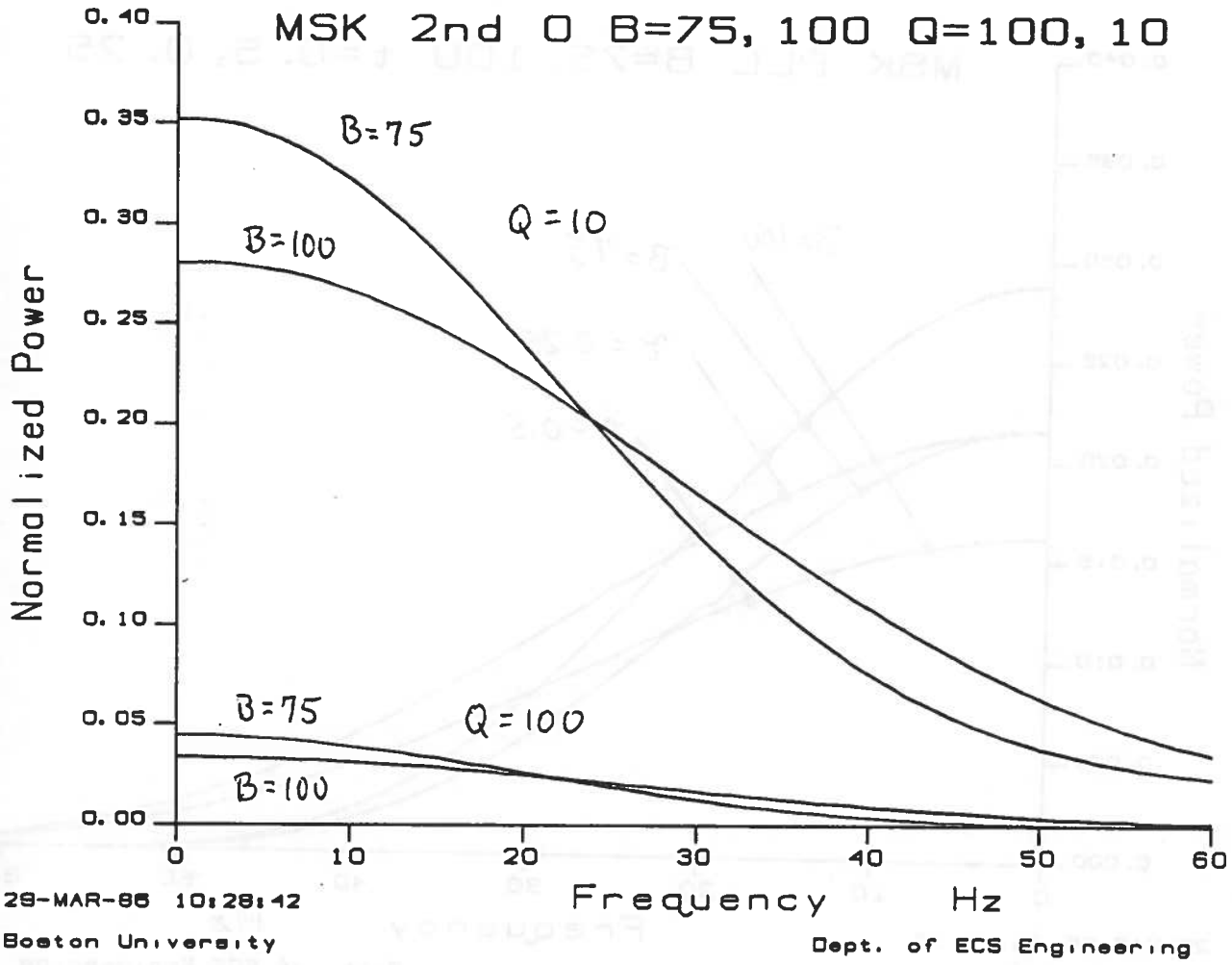

Figure 2.19: P_{filter} for 2nd Order ADF

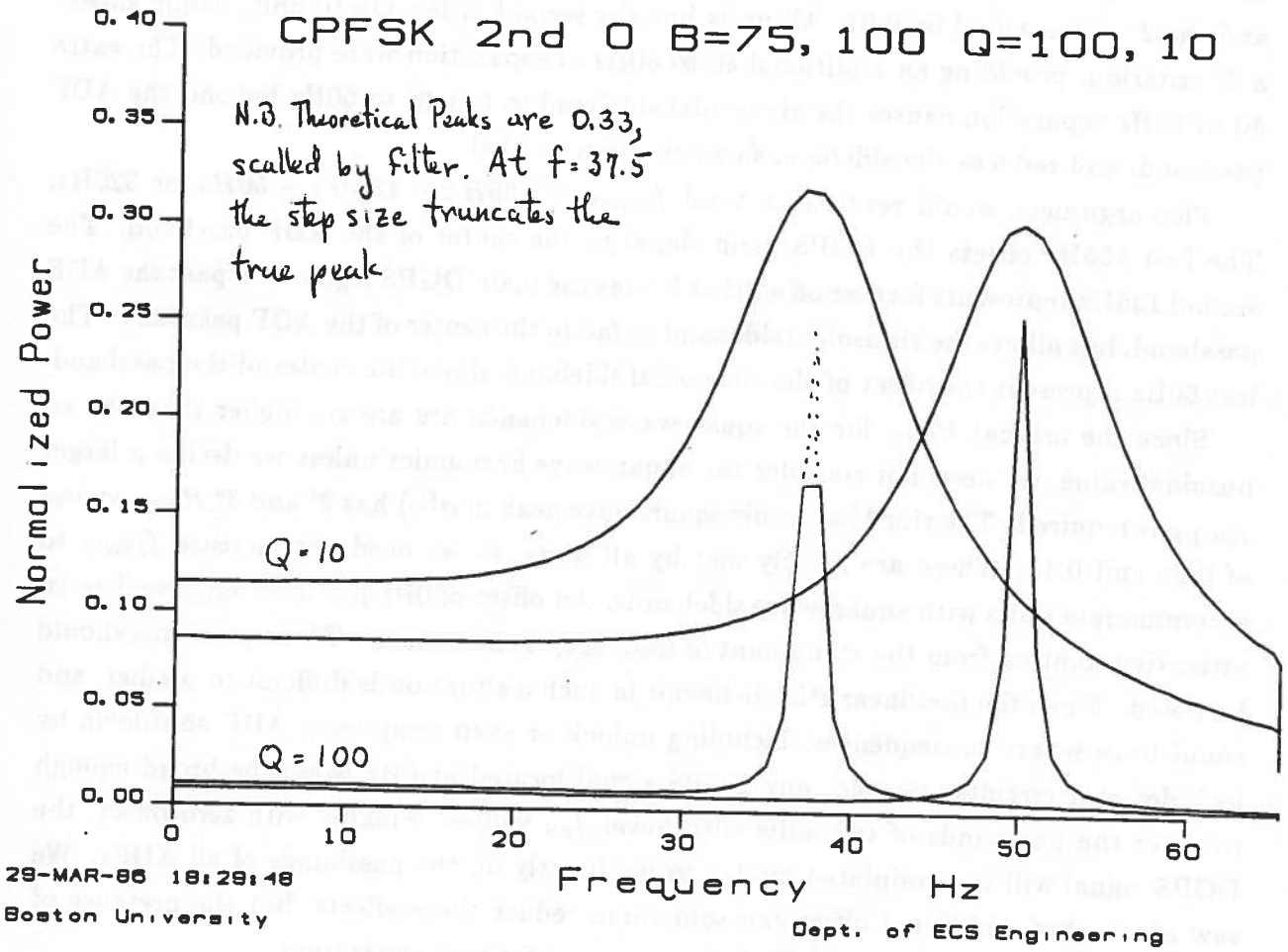

Figure 2.21: P_{filter} for CPFSK in 2nd Order ADF

squarewave harmonic would create 3° or more bearing error.

2.8 Conclusions

Based on the above analysis, we make the following recommendations:

1. Modulation should be MSK. CPFSK, with its discrete frequency components, is subject to P_{filter} values near 0.3, and could produce unacceptably large $\sigma(\hat{\phi})$ even at large offsets due to its DGPS sidebands having discrete components.

2. Offset should be greater than 325Hz. One unit with $f_{SS} = 200Hz$ and second order units with low Q might experience errors greater than 3° for this offset. However, such units are apparently out of production or of comparatively low quality. An offset to include these units would have to be between 450 and 600Hz.

3. DGPS protection ratio should be -3dB. A -6dB ratio would still require an offset sufficient to reach the sinusoidal sideband. Going to -6dB would only reduce the need to slide somewhat beyond the sinusoidal sideband, changing the total offset from say 325 to 275Hz.

4. Symbol rate should be 100 symbols per second (rate 1/2 coding). This serves to spread the energy in the spectra, and reduces $\sigma(\hat{\phi})$. For a given ADF, this reduction occurs because the DGPS interference spectrum is widened compared to the ADF passband. It also improves the range of the DGPS transmission, as discussed in section 3.

Two major concerns should be mentioned. First, there may be further ADFs that we did not encounter in our survey. If their characteristics differed greatly, the conclusions might need revision. The conservative worst case approach employed here makes it unlikely that any ADFs will have significantly different interference characteristics from those seen here. Second, a linear analysis is only approximate for ADFs. It is suggested that bench testing be performed on at least a subset of ADFs to ensure that nonlinearities do not degrade ADF performance in the presence of DGPS.

in section 3.6. It assumes that the noise power, skywave amplitude and skywave phase are fixed, and it results in a family of curves, which give probability of bit error versus signal to noise ratio.

Section 3.4 computes the probability of link availability, which is defined as the probability that the SNR required for $Pr(\epsilon) \leq 10^{-5}$ is achieved. As such, $Pr(link\ available) = 1 - Pr(outage)$. This portion of our overall analysis incorporates the variation of the noise power, skywave amplitude and phase as described in [4], [5], [6], and [13].

Section 3.5 presents and discusses the combined results of sections 3.3 and 3.4. It gives the range to which the link will be available with probability 0.90 under "worst case" conditions in Boston, Massachusetts.

Finally, section 3.6 considers the burst nature of atmospheric noise and the techniques which must be used to overcome these bursts.

3.2 Error Detecting and Correcting Codes

In the sections that follow, we will show that error detecting and correcting (EDAC) codes greatly enhance the performance of the radiobeacon-DGPS link. In this section, we briefly introduce coding and its associated terminology. Error correction coding is essentially a signal processing technique used to improve the reliability of communication on digital channels. Even though specific coding techniques differ widely in their details, they all share the fundamental features depicted in Figure 3.1.

As shown, the data sequence is broken into vectors of length k. There are 2^k such data vectors and the code maps each of these into a unique n-tuple (a vector of length n) and these n-tuples are known as codewords. For each codeword, there are 2^{n-k} n-tuples with no corresponding data vector. A good code is designed such that these extra n-tuples form buffer zones around the codewords. Consequently, many channel errors must occur before a given codeword is confused with an n-tuple from another codeword's buffer zone. Good codes have a large distance between all codewords in the code. The most common measure of distance is Hamming distance, which is the number of places in which the two codewords differ.

There are two classes of codes:

- block codes
- convolutional codes

In this report, we consider convolutional codes only and a convolutional encoder is shown in Figure 3.2. As shown, two new information bits are input to the encoder in each cycle and three channel symbols are output from the encoder in each cycle. Consequently,

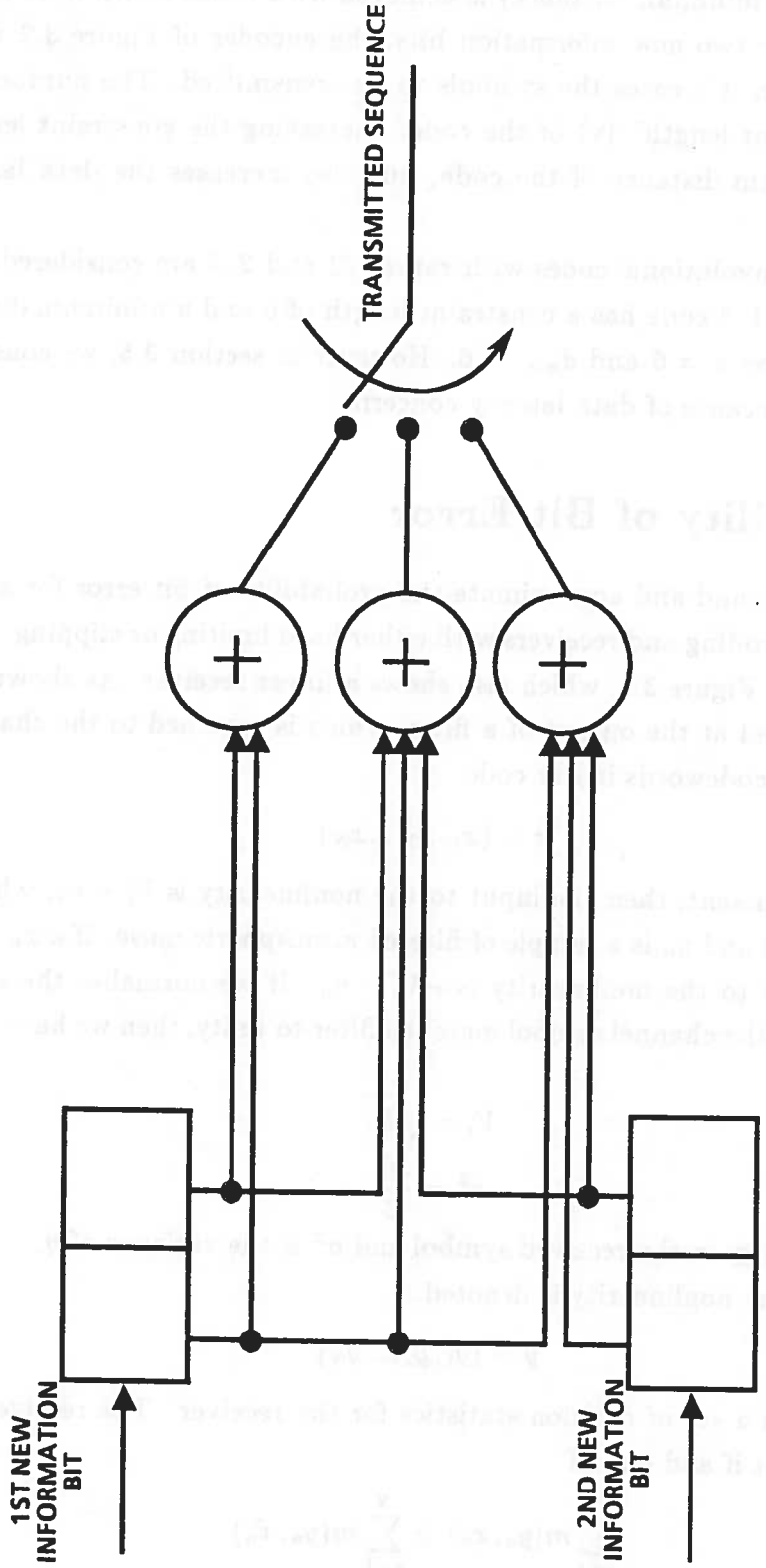

Figure 3.2: Convolutional Encoder for Code with R=2/3 and v=2, k=4

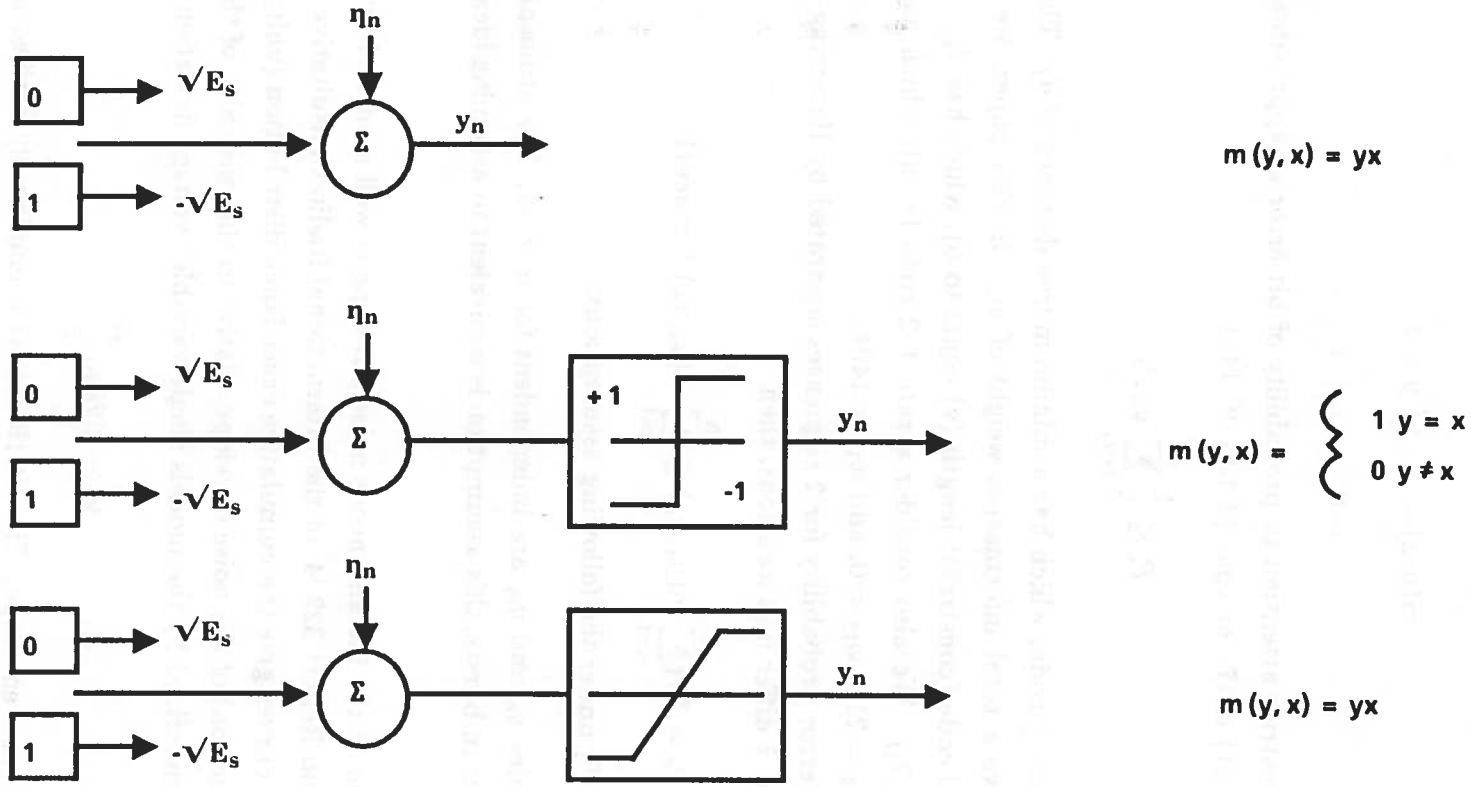

Figure 3.3: Channel/Receiver Models

Rayleigh" ([12]) and a computer program (APDAN) exists ([1]), which returns values of the exceedance distribution for a given value of envelope and voltage deviation. We have modified APDAN so it also returns the envelope density function ($f_R(r)$) and we use this feature extensively in what follows.

- Finally we assume that the skywave/groundwave interference is such that the fade depth is constant. This assumption is reasonable, because the skywave phase and amplitude have a long correlation time (tens of minutes) at LF and lower MF frequencies.

With independent noise samples (η_n) we may apply the Chernoff bound to equation (2)

$$P_d \leq \min_{\lambda \geq 0} \prod_{n=1}^{N} E(exp\lambda(m(y_n, \hat{x}_n) - m(y_n, x_n)) \mid x_n)$$

If we define

$$D = \min_{\lambda \geq 0} E(exp\lambda(m(y_n, \hat{x}_n) - m(y_n, x_n)) \mid x_n)$$

$$= \min_{\lambda \geq 0} D(\lambda)$$

then, we have

$$P_d \leq D^{w_H(x,\hat{x})} \tag{3.3}$$

where $w_H(x, \hat{x})$ is the Hamming distance between x and $\hat{x}$.

For a hard limiter,

$$D = \sqrt{4\epsilon(1-\epsilon)} \tag{3.4}$$

where

$$\epsilon = Pr(\eta \geq \sqrt{E_s})$$

We can compute ϵ as a function of the envelope density provided by APDAN by using a result from [12]

$$\epsilon = \frac{1}{\pi} \int_{\sqrt{E_s}}^{\infty} p_R(r) cos^{-1}\left(\frac{\sqrt{E_s}}{r}\right) dr \tag{3.5}$$

For a clipper, we have

$$D(\lambda) = E(exp\lambda(\hat{x}_n y_n - x_n y_n) \mid x_n)$$

$$= E(exp\lambda y_n(-2\sqrt{E_s}))$$

For simplicity, we consider a piecewise constant clipper with $2I+1$ pieces and which clips at $y = clip\sigma_\eta$. In this case

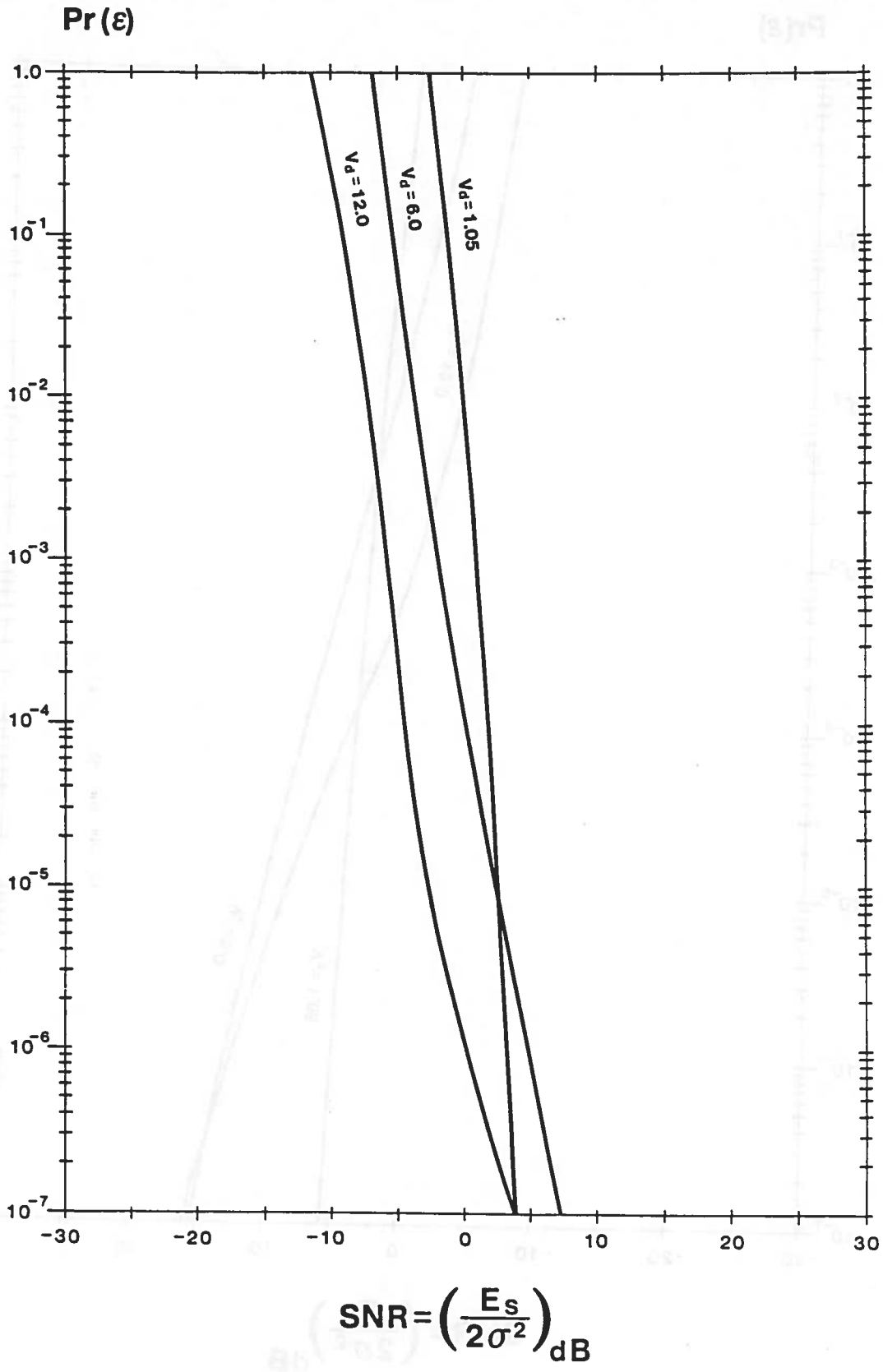

Figure 3.4: Chernoff Bound, Rate 1/2 Convolutional Code, Clipping Receiver (Clip = 1σ)

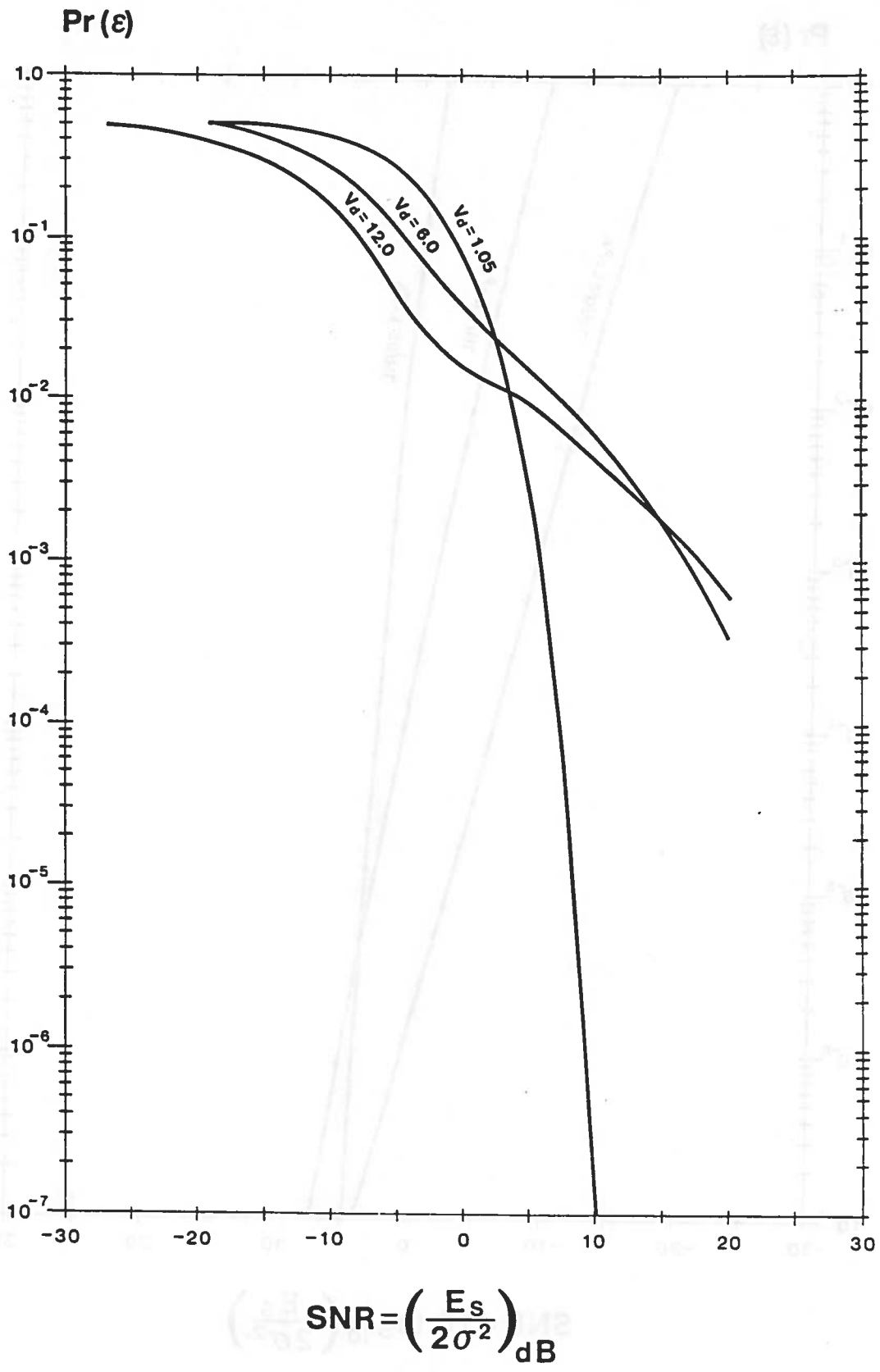

Figure 3.6: Chernoff Bound, Rate 1/2 Repetition Code, Clipping Receiver (Clip = 1σ)

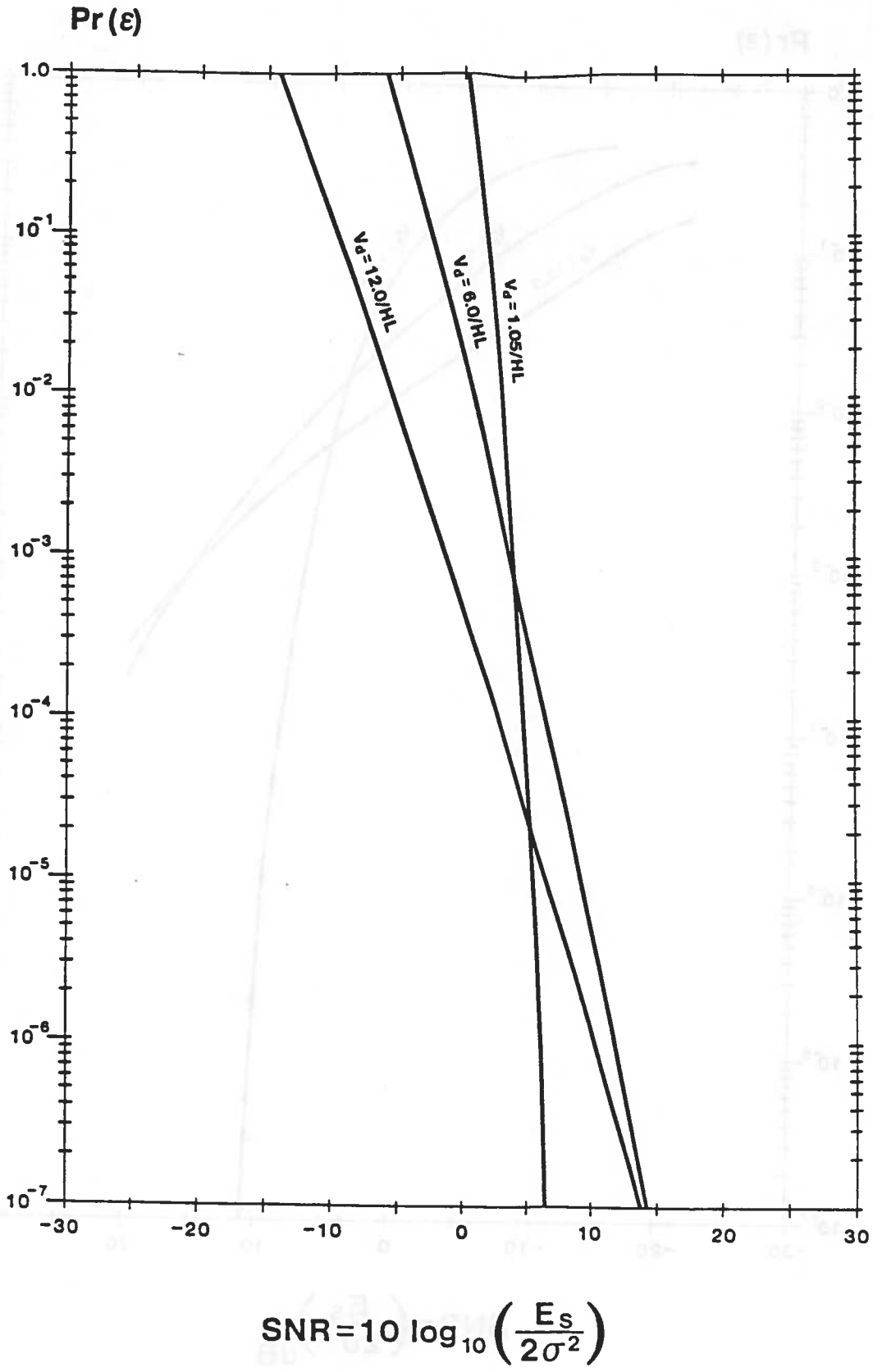

Figure 3.8: Binomial Distribution, Rate 2/3 Convolutional Code, Hard Limiting Receiver

frequency. For a given season-time block, the variation of measured noise power (in decibels) away from the average noise power is adequately represented by a two-sided Gaussian distribution. For values of noise power below the average noise power, one standard deviation ($\sigma_{\eta,l}$) applies and for values of noise power above the average another standard deviation ($\sigma_{\eta,u}$) applies. Both $\sigma_{\eta,l}$ and $\sigma_{\eta,u}$ can be computed using the NTIA Report.

- Groundwave field strength is accurately predicted using the curves in [3]. These curves give field strength versus distance with center frequency and ground conductivity as parameters. The example curves we present later assume a center frequency of 300 kHz and propagation over seawater.

- Skywave field strength is accurately modelled by the techniques summarized in CCIR Report 575-1. These methods use the following form for the median skywave field strength

$$\overline{S}(dB\ above\ 1\mu V/m) = C - s(d) + P + \triangle_A - \triangle_t$$

where C is a constant which depends on the prediction method used and $s(d)$ gives distance dependence. P is a correction for transmitters which radiate other than 1kW and the $\triangle_k$ belong to set of correction factors. In our case, we use the correction factors for the vertical directivity of the transmitting antenna ($\triangle_A$) and time of day ($\triangle_t$). The distribution of skywave field strength away from its median may be estimated by using a set of curves in [5]. For the times when the median skywave is strong, we find that the distribution of skywave strength (in decibels) is well approximated by another 2-sided Gaussian distribution. In other words, 2 standard deviations ($\sigma_{S,u}\ and\ \sigma_{S,l}$) will approximately characterize the random variations of skywave at a given time.

- Finally, we assume that the relative phase of the received groundwave and skywave is uniform on $[0, 2\pi)$. This assumption seems reasonable at 300 kHz where the wavelength (1000 *meters*) is reasonably small compared to the irregularites in ionospheric height.

In the case of groundwave only propagation, we can write

$$Pr(linkavailable) = Pr(SNR \geq k) = Pr(\frac{E_s}{N_o} \geq k)$$

$$= Pr(E_{n,dB} \leq -k_{dB} + G_{dB} + P) \tag{3.7}$$

where $E_{n,dB}$ is the noise power in decibels above $1\mu V/m$. k_{dB} is the required signal to noise ratio from Figures 3.4 through 3.9. G_{dB} is the groundwave power for a radiated power of

where we have approximated an integral by a sum. The first term in the above sum can be written as

$$Pr(SNR > k \mid f_{i,dB} - \triangle < F_{dB} \leq f_{i,dB} + \triangle)$$
$$\approx Pr(E_{n,dB} \leq -k_{dB} + G_{dB} + P + f_{i,dB}) \tag{3.10}$$

Unfortunately, the second term in the above sum requires more work.

$$Pr(f_{i,dB} - \triangle < F_{dB} \leq f_{i,dB} + \triangle)$$
$$= P_F(10^{(f_{i,dB}+\triangle)/20}) - P_F(10^{(f_{i,dB}-\triangle)/20}) \tag{3.11}$$

where $P_F(f) = Pr(F < f)$ is the distribution function of F. With $F = \mid 1 + \hat{S}cos\theta \mid$, we find

$$P_F(f) = \int_D \int p_{\hat{S},\theta}(\hat{S},\theta) d\hat{S} d\theta$$

where D is the region where $\mid 1 + \hat{S}cos\theta \mid \leq f$. After some algebra, we find that if f is less than one, then

$$P_F(f) = \frac{1}{\pi} \int_{\pi/2}^{\pi} P_{\hat{S},dB}(20log_{10}(\frac{1+f}{-cos\theta})) - P_{\hat{S},dB}(20log_{10}(\frac{1-f}{-cos\theta}))d\theta \tag{3.12}$$

where $P_{\hat{S},dB}$ is a two sided Gaussian distribution.

$$P_{\hat{S},dB}(x) =$$

$$1 - Q\left(\frac{x - \overline{S}_{dB} + G_{dB}}{\sigma_{s,l}}\right) \quad if\ x \leq \overline{S}_{dB} - G_{dB}$$

$$1 - Q\left(\frac{x - \overline{S}_{dB} + G_{dB}}{\sigma_{s,u}}\right) \quad if\ x > \overline{S}_{dB} - G_{dB}$$

If f is greater than 1, then

$$P_F(f) = \frac{1}{\pi} \int_0^{\pi/2} P_{\hat{S},dB}(\frac{f-1}{cos\theta})d\theta + \frac{1}{\pi} \int_{\pi/2}^{\pi} P_{\hat{S},dB}(\frac{f+1}{-cos\theta})d\theta \tag{3.13}$$

Equations (3.8) through (3.13) have been used to generate Figures 3.10 through 3.20, and these Figures are parameterized by the quantity $k_{dB} - P$.

As shown, as $k_{dB} - P$ increases the range of reliable communication decreases. This is reasonable, because increasing k_{dB} means the required signal to noise ratio is increasing. Decreasing P means that less power is being radiated relative to 1 kW. The Figures show separate curves for groundwave only propagation and combined groundwave/skywave propagation. As shown, groundwave only propagation would give more reliable service at short and medium ranges, but would give less reliable service for longer ranges. The combined propagation modes do result in possible fading effects at medium ranges. Figures 3.10 through 3.20 are further discussed in the next section.

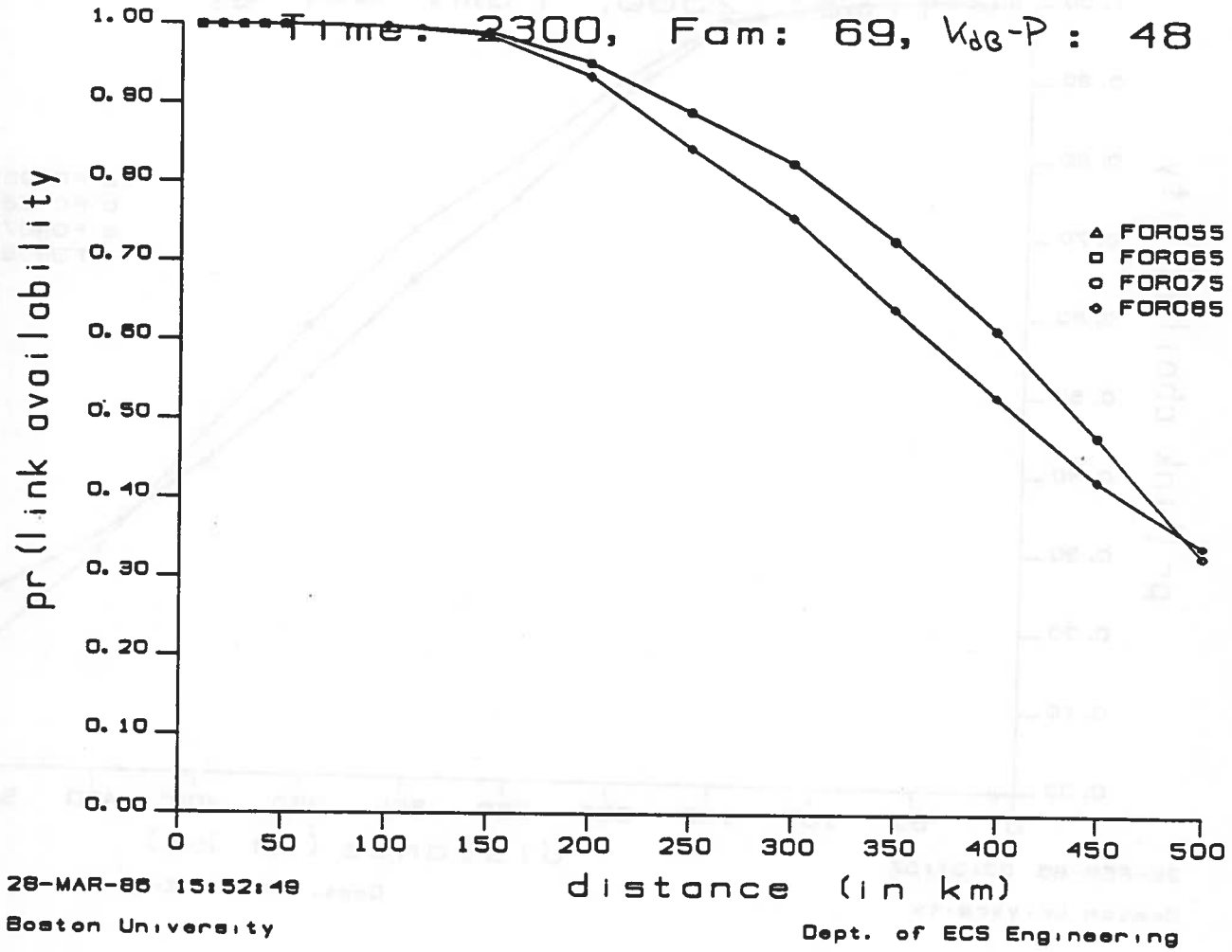

Figure 3.11: Pr(Link Availability) for 2300 hr, $F_{am} = 69$, and $k_{dB} - P = 48$

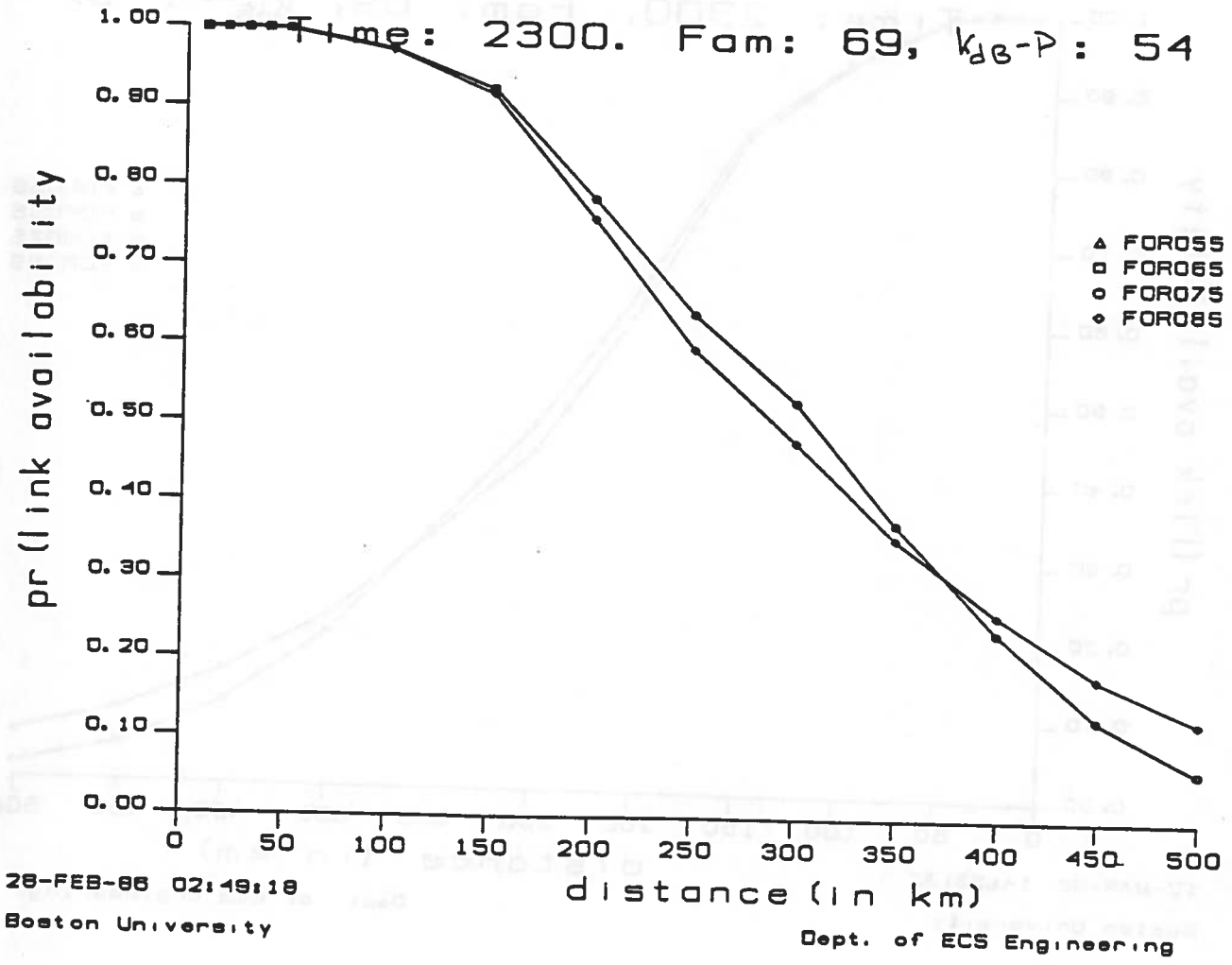

Figure 3.13: Pr(Link Availability) for 2300 hr, $F_{am} = 69$, and $k_{dB} - P = 54$

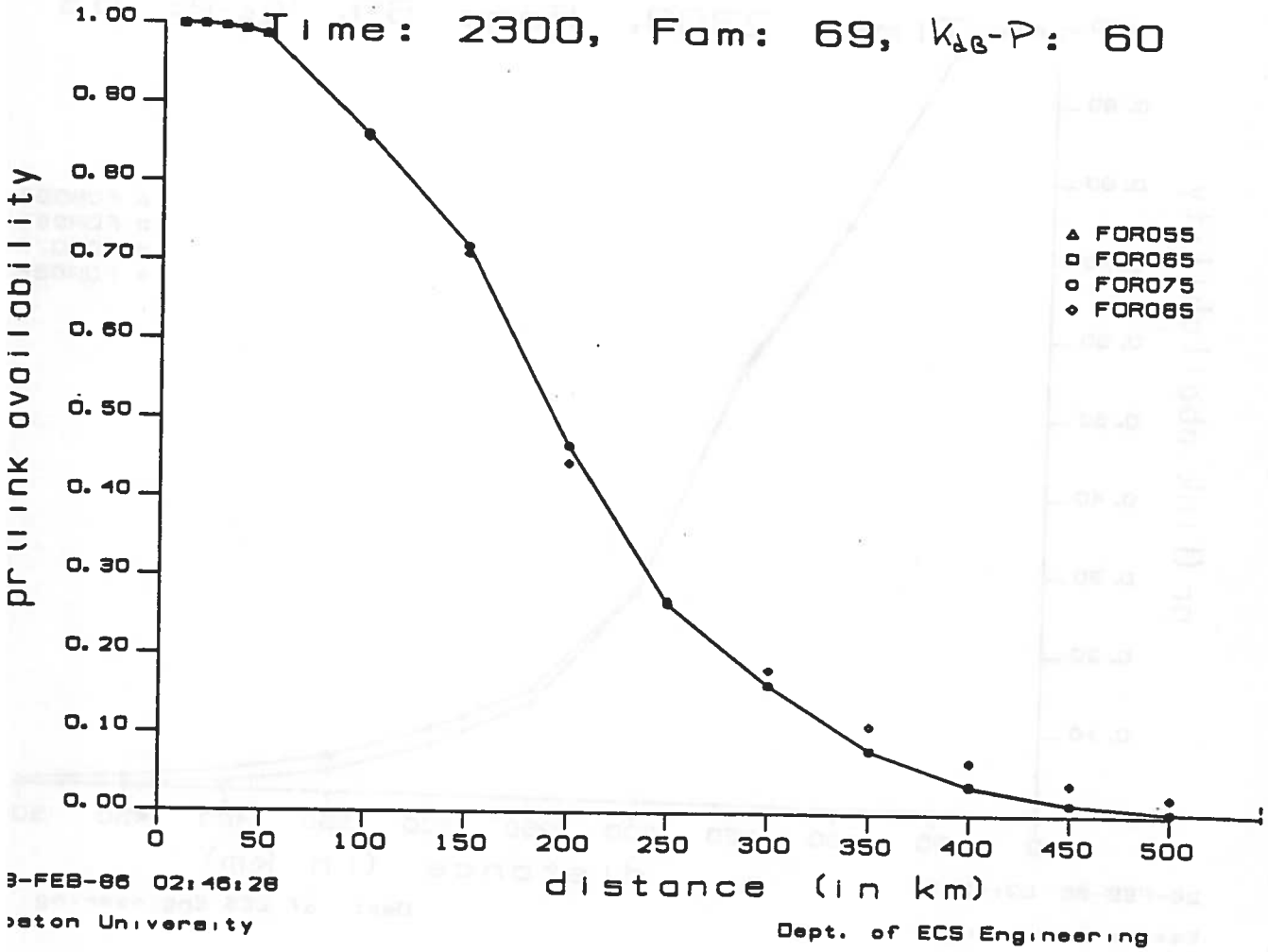

Figure 3.15: Pr(Link Availability) for 2300 hr, $F_{am} = 69$, and $k_{dB} - P = 60$

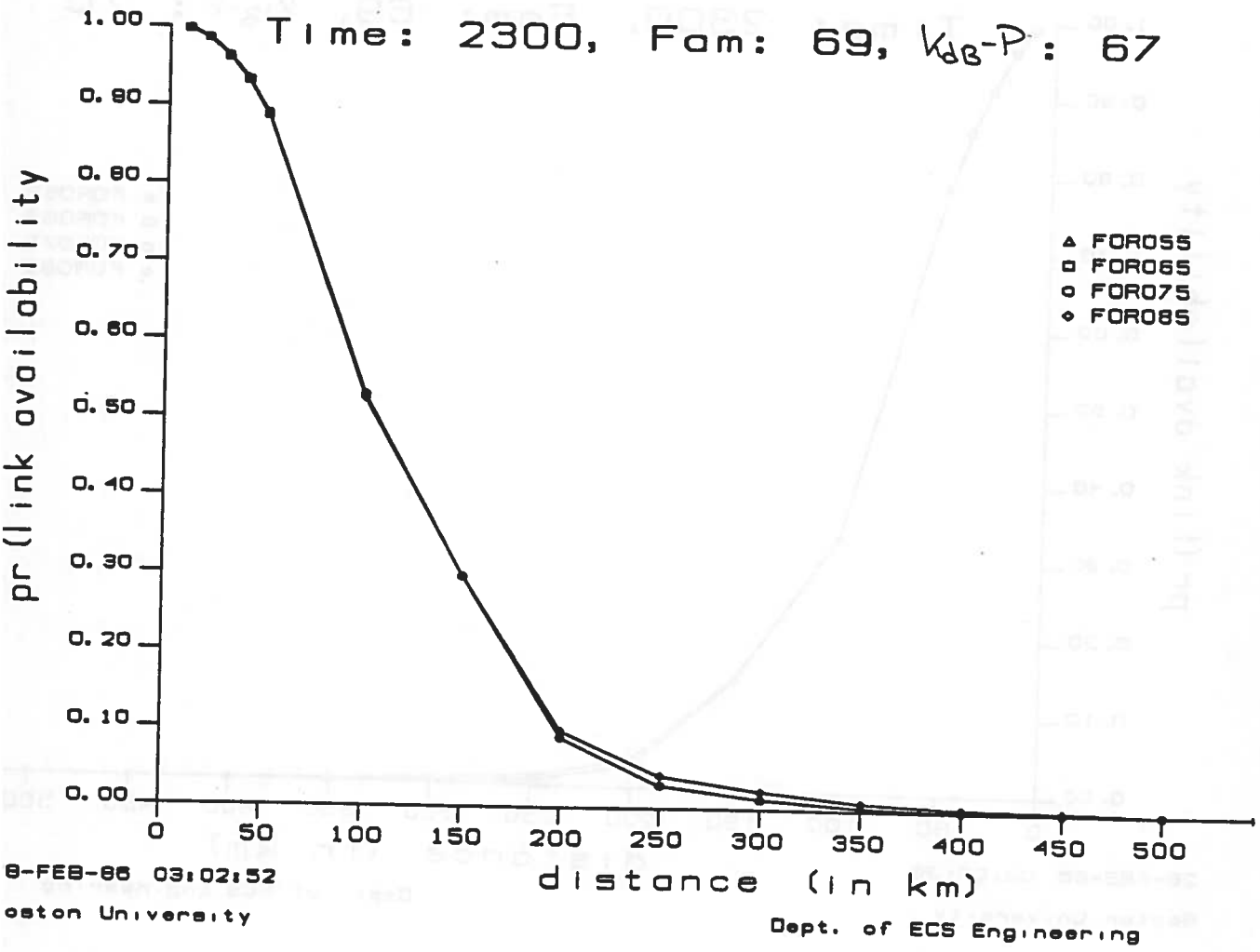

Figure 3.17: Pr(Link Availability) for 2300 hr, $F_{am} = 69$, and $k_{dB} - P = 67$

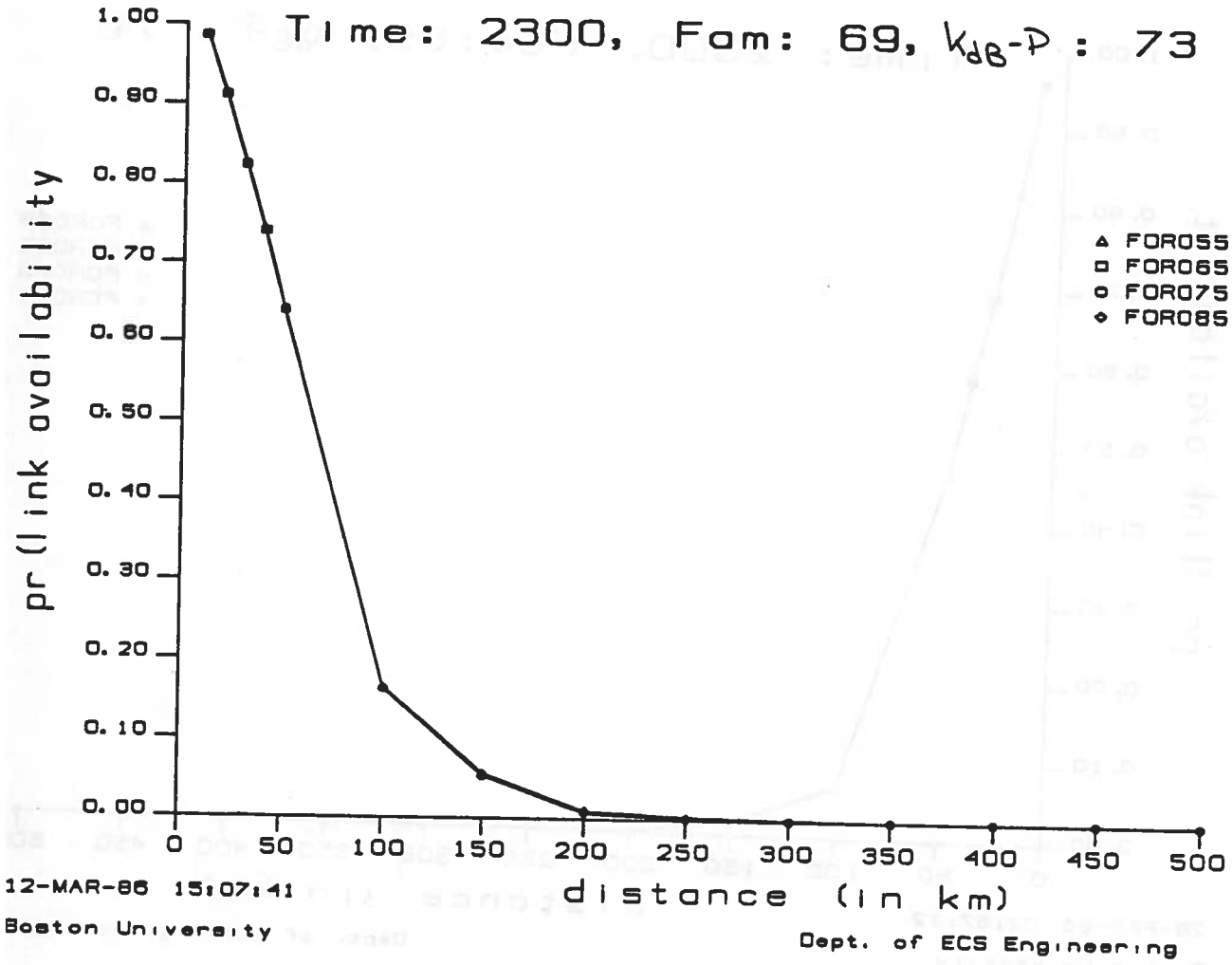

Figure 3.19: Pr(Link Availability) for 2300 hr, $F_{am} = 69$, and $k_{dB} - P = 73$

3.5 Numerical Results and Discussion

The main results of Chapter 3 are given in Table 3.1. which shows the range to which a link will be available with probability 0.90 under "worst case" conditions in Boston, Massachusetts. In Boston, worst case conditions occur summer nights near midnight, because the mean atmospheric noise power is greatest and skywaves are strongest. Table 3.1 gives the 90 percent range for no coding, the rate 1/2 (v=6) and rate 2/3 (v=6) codes. As shown, the uncoded system performs very poorly when the noise power is high. However, the coded systems have much greater operating ranges. Remember, atmospheric noise power is very variable and most of the time any of the systems will have much greater ranges.

Table 3.1: Beacon Ranges with and without Coding

	10 nautical mile beacon		30 nautical mile beacon	
	$k_{dB} - P$	Range	$k_{dB} - P$	Range
No Coding				
Limiter	84 (dB)	$\leq 10km$	75 (dB)	15 (km)
Clipper	84	$\leq 10km$	75	15
Rate 1/2, v=6				
Limiter	59	100	50	195
Clipper	58	110	49	210
Rate 2/3, v=6				
Limiter	65	55	56	130
Clipper	66	50	57	120

The table was derived using the following procedure.

1. The required signal to noise ratio for $Pr(\epsilon) \leq 10^{-5}$ is determined for hard limiters and clippers from Figures 3.4 through 3.9. For hard limiters, these SNRs are 28, 9, and 3 dB for no coding, rate 2/3 coding and rate 1/2 coding. For clippers these SNRs are 28, 10, and 2 dB. To these values we add a 3 dB "pad" to account for departures from the ideal conditions used in the analysis. These required SNRs are represented as k_{dB} in equations (7) and (10).

2. The term P in equations (7) and (10) is the radiated power of the beacon relative to 1kW. The radiated power of a beacon is indirectly specified. A "30 nautical mile" beacon produces a field of $50\mu V/m$ at a range of 30 nm over seawater. A "10 nautical

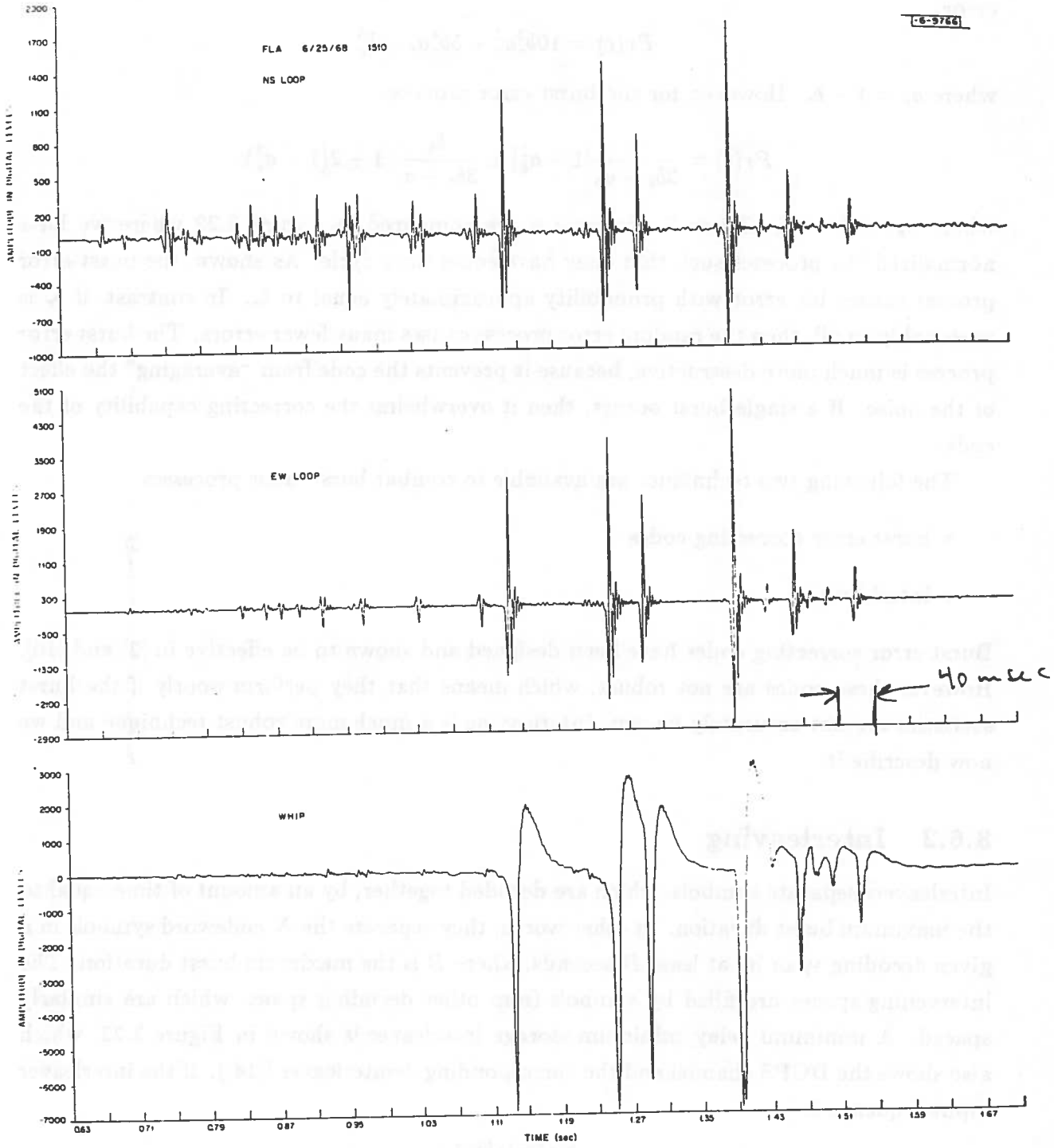

Figure 3.21: ELF Waveforms Recorded in Florida (June 1968)

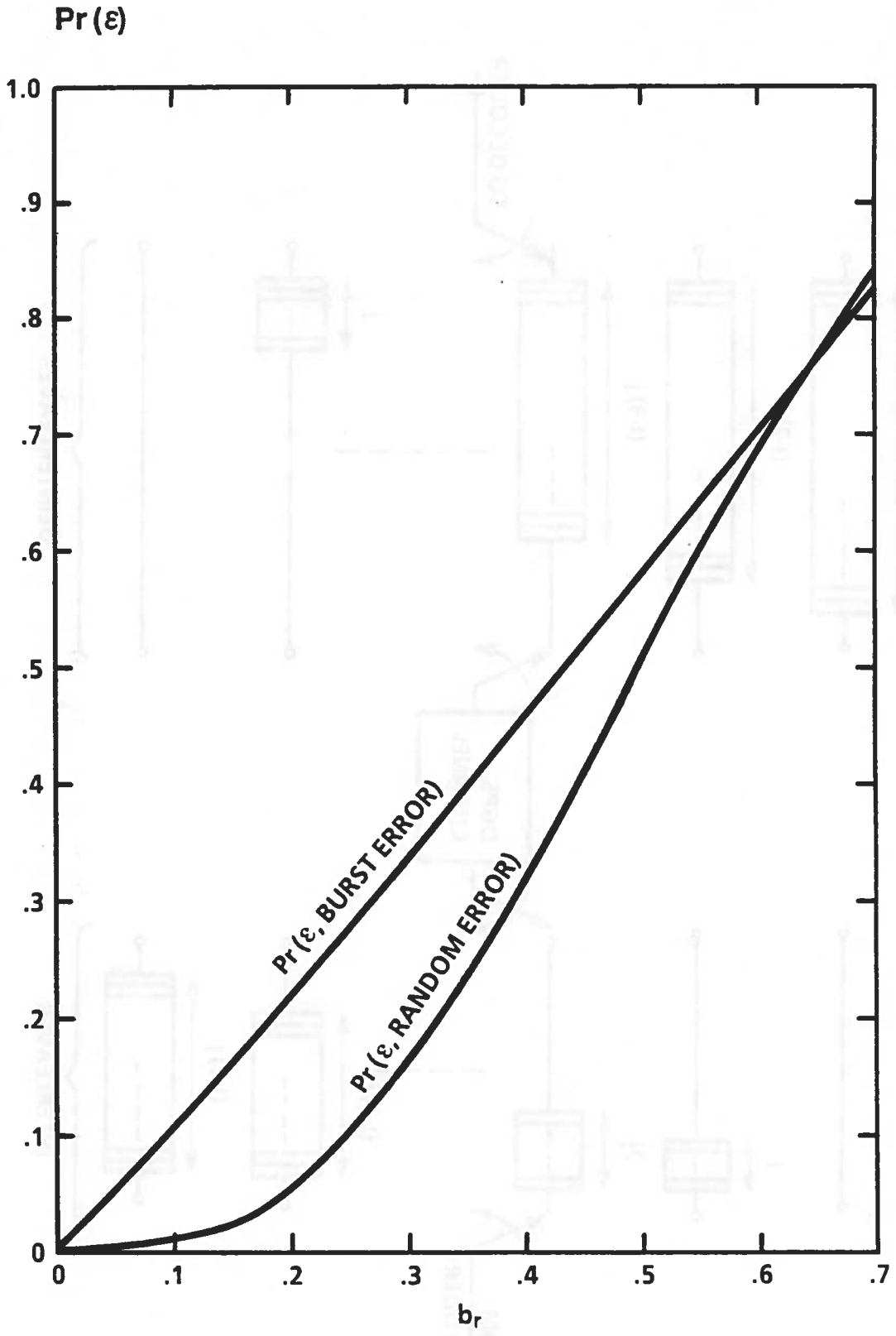

Figure 3.22: Pr(Bit Error) vs. Burst Error and Random Error Processes

If input symbols have separation less than $J = jI$, then they will have minimum channel transmission separation of I. Consequently, the interleaver of Figure 3.23 is known as a $(I.J)$ interleaver. We should select J and I such that all symbols which are decoded together will be separated by B seconds. Consequently, J should be at least equal to the codeword length if block codes are used or the "decoding span" if convolutional codes are used. I should be equal to the maximum burst length in channel symbols (B/T_c).

The delay introduced by this (I, J) interleaver is $J(I-1)T_c$ or approximately NB, where N is either codeword length or decoding span. To determine delay, we need values for N and B and we now consider those topics in turn.

3.6.3 Decoding Span (N)

The decoding span of a convolutional code depends on the constraint length of the code and the type of decoder used. There are 3 classes of convolutional decoders.

- Viterbi decoding
- syndrome decoding
- sequential decoding

The decoding span for Viterbi decoders may be estimated using the following rules of thumb. If the code has $R = 1/2$ and constraint length equal to v, then $N = 5v/R$ channel symbols. If the code has $R = 2/3$, then $N = 8v/R$ channel symbols and if $R = 3/4$, then $N = 10v/R$.

Syndrome decoders can have much shorter decoding spans, but achieve this reduction by sacrificing some of their error correcting capability. This tradeoff will be investigated in Technical Task No. 2.

Sequential decoders are generally used with codes which have much greater constraint lengths ($v \geq 20$) than the codes considered in this Report. Nonetheless, they will be studied in Technical Task No. 2.

3.6.4 Atmospheric Burst Duration (B)

Atmospheric burst duration has been measured by [8], [9], and [11], and in this subsection we summarize the observations made by J. Evans ([8]). Evans defined x as the length of the interval between bursts and used noise data from Florida to compute

- the sample probability density function of x $(p_X(x))$
- the sample "survivor function" of x $(R(x))$. $R(x)$ is the fraction of burst intervals greater than x. So $R(x) = \int_x^\infty p_X(u)du$

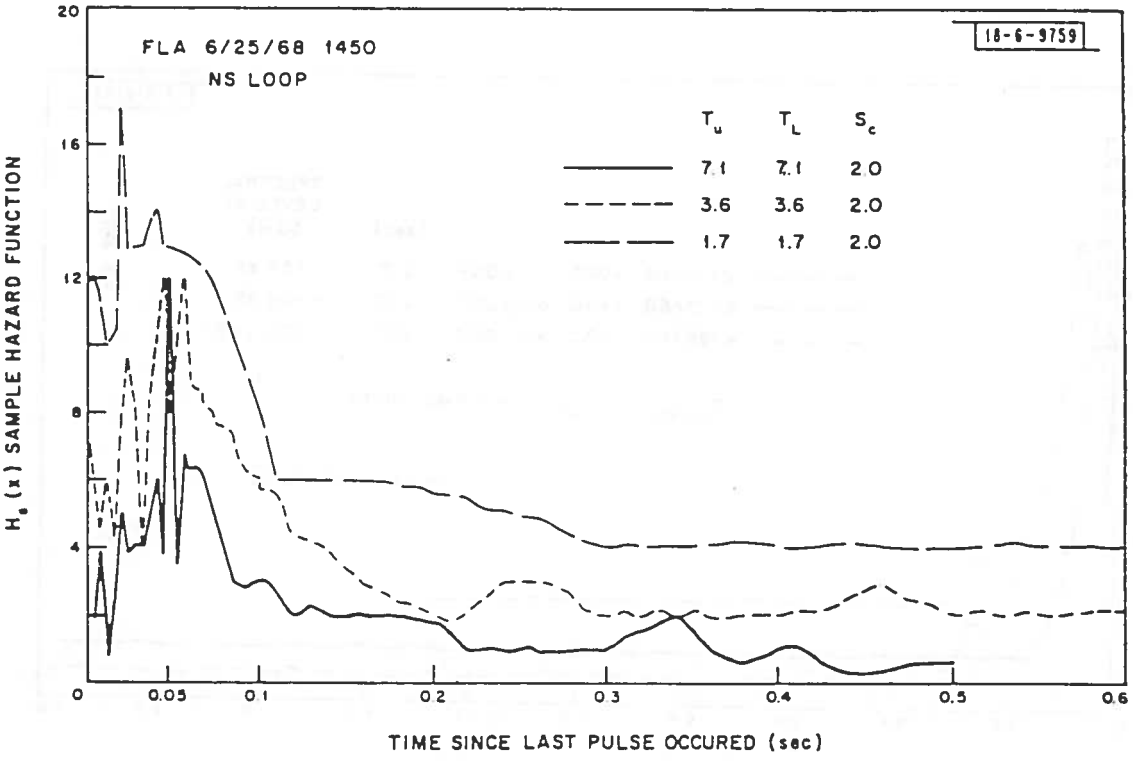

Figure 3.24: Hazard Function of Interburst Interval for Various Criteria (Florida, June 1968)

Bibliography

[1] H. Akima, "A Method of Numerical Representation for the Amplitude Probability Distribution of Atmospheric Radio Noise," U.S. Dept. of Commerce, Office of Telecommunications, OT/TRER 27, 1972

[2] K. Brayer, "Error Correcting Code Performance on HF, Troposcatter, and Satellite Channels," IEEE Trans. on Commun. Tech., vol COM-19, pp 835-848

[3] CCIR, "XIth Plenary Assembly Oslo, Vol II: Propagation," International Telecommunication Union (ITU), Geneva, 1966, pp 42-51

[4] CCIR (International Radio Consultative Committee) Report 322, "World Distribution and Characteristics of Atmospheric Radio Noise," International Telecommunication Union (ITU), Geneva, 1964

[5] CCIR Recommendation 435-3, "Prediction of Sky-Wave Field Strength Between 150 and 1600 kHz," ITU, Geneva, 1978

[6] CCIR Report 575-1, "Methods for Predicting Sky-Wave Field Strengths at Frequencies Between 150 kHz and 1600 kHz," ITU, Geneva, 1978

[7] G.C. Clark and J.B. Cain, "Error Correction Coding for Digital Communication," Plenum, New York, 1981

[8] J.E. Evans, "Preliminary Analysis of ELF Noise," Lincoln Laboratory Technical Note 1969-18, March 1969

[9] S. Gupta, "Short Term Time Characteristics of Atmospheric Radio Noise Above Different Thresholds," IEEE Trans. EMC, vol. EMC-13, No. 4, Nov. 1971

[10] A. Kohlenberg, and G. Forney, "Convolutional Coding for Channels with Memory," IEEE Trans. Info. Theory, vol. IT-14, pp 616-626